Aggregation dynamics and identification of aggregation-prone mutants of the von Hippel-Lindau tumor suppressor protein

Xavier Le Goff, Franck Chesnel, Olivier Delalande, Anne Couturier, Stephane Dréano, Cathy Le Goff, Cécile Vigneau, Yannick Arlot-Bonnemains

HAL Id: hal-01357624
https://univ-rennes.hal.science/hal-01357624

Aggregation dynamics and identification of aggregation-prone mutants of the von Hippel Lindau tumor suppressor protein

Xavier Le Goff[1*], Franck Chesnel[1], Olivier Delalande[1], Anne Couturier[1], Stéphane Dréano[1], Cathy Le Goff[1], Cécile Vigneau[1,2] and Yannick Arlot-Bonnemains[1]

1 CNRS, UMR 6290 IGDR, Université Rennes 1, BIOSIT, Rennes, France
2 CHU Rennes, service de néphrologie, Rennes, France

* Corresponding author
E-mail: xavier.le-goff@univ-rennes1.fr

Summary statement

If misfolded, the von Hippel Lindau (pVHL) tumor suppressor is prone to aggregate and to be degraded. Tumorigenic mutations may compromise its folding. We identified new factors regulating pVHL folding.

Abstract

Quality control mechanisms promote aggregation and degradation of misfolded proteins. In budding yeast, the von Hippel Lindau protein (pVHL) is misfolded and forms aggregates. Here we investigated the aggregation of three pVHL isoforms (pVHL213, pVHL160, pVHL172) in fission yeast. The full length pVHL213 isoform aggregates in highly dynamic small puncta and in large spherical inclusions, either close to the nucleus or to the cell ends. The large inclusions contain the Hsp104 chaperone. Aggregate clearance is regulated by proteasomal degradation. The pVHL160 isoform forms dense foci and large, irregularly shaped aggregates. *In silico* prediction of pVHL aggregation propensity identified a key aggregation-promoting region within exon 2. Consistently, the pVHL172 isoform, which lacks exon 2, formed rare reduced inclusion. We studied the aggregation propensity of pVHL variants harboring missense mutations found in kidney carcinomas. We showed that the P86L substitution stimulated small aggregate formation, the P146A mutation increased large inclusion formation while I151S destabilized pVHL. The prefoldin subunit Pac10 (the human homolog VBP-1 binds to pVHL) is required for pVHL stability. Reduction of soluble functional pVHL may be critical in VHL-related diseases.

Introduction

The human VHL gene encodes three different isoforms from two transcripts: the mRNA variant 1 encodes the full length pVHL213, which includes a hydrophobic β domain and a hydrophobic α domain, and a shorter pVHL160 version produced from an internal translation start site. The mRNA variant 2 encodes pVHL172 in which exon 2 is excluded by an alternative splicing event. We recently showed that these isoforms are co-expressed in human renal cells (Chesnel et al., 2015). Mutations in the von Hippel Lindau (*VHL)* gene cause the von Hippel Lindau (VHL) disease, an inherited cancer syndrome in which highly vascularized tumors, such as clear cell carcinoma, hemangioblastoma and pheochromocytoma (Latif et al., 1993; Richard et al., 2013), are frequently observed. The human pVHL protein acts as a tumor suppressor and is mutated in 80% of sporadic clear cell renal carcinoma (ccRCC). pVHL is a component of the E3 ubiquitin ligase complex VBC that includes also elongins B and C (ELOB and C), cullin-2 and RBX1. The VBC complex regulates the cellular response to oxygen concentration by targeting the transcription factor HIFα for proteasomal degradation (Kamura et al., 2000).

In eukaryotes, 20-30% of proteins adopt folded conformations only after interaction with binding partners (Tyedmers et al., 2010). In the absence of partners, proteins may be misfolded and incorporated into aggregates. Full length pVHL (pVHL213; 213 amino acids) is an aggregation-prone protein (Shmueli et al., 2013). When properly folded after sequential interaction with the HSP70 chaperone and the TRiC chaperonin, pVHL binds to ELOB or C to form the VBC complex (Feldman et al., 2003; Feldman et al., 1999; McClellan et al., 2005; Melville et al., 2003). Misfolded pVHL cannot bind to ELOC/ELOB and is degraded by a pathway involving the HSP90 chaperone (McClellan et al., 2005; Schoenfeld et al., 2000). pVHL mutations detected in ccRCC may compromise its native folding and conformation and alter its binding to TRiC (Feldman et al., 2003; Feldman et al., 1999).

The budding and fission yeast expression systems allow studying the mutation-driven aggregation properties of a given protein and identifying molecular pathways involved in the cellular fate of proteins by genetic screens (Summers and Cyr, 2011). Human pVHL213 expressed in budding yeast does not fold properly because its cognate human partners are not endogenously expressed. Instead, it aggregates in two different subcellular compartments: Insoluble Protein Deposit (IPOD), which is close to the vacuole, and JUxtaNuclear Quality control compartment (JUNQ). There, aggregated proteins are either refolded by chaperones, or degraded by the proteasome (Kaganovich et al., 2008; Specht et al., 2011). Moreover, a new intra-nuclear inclusion (INQ) has been described recently, for the deposition of nuclear and cytosolic misfolded proteins (Miller et al., 2015). The Hsp104 chaperone binds stress-induced protein aggregates nonspecifically. In yeast, stress-induced misfolded proteins first accumulate as stress foci or Q bodies, prior to Hsp104-dependent fusion

with IPOD or JUNQ (Escusa-Toret et al., 2013; Spokoini et al., 2012). In mammalian cells, excess of misfolded protein are incorporated in JUNQ or IPOD, depending on the nature of the misfolded protein. Specifically, overexpressed pVHL is essentially found in JUNQ in different mammalian cell lines (Ogrodnik et al., 2014; Weisberg et al., 2012).

Ubiquitination is a key regulatory mechanism to sort misfolded proteins. Ubiquitinated and soluble proteins are found in the JUNQ, where they can rapidly transit back to the cytosol. Conversely, terminally aggregated insoluble proteins are incorporated in the IPOD and targeted for degradation (Kaganovich et al., 2008). However, the exact role of ubiquitination in targeting misfolded pVHL in specific inclusions has been questioned (Miller et al., 2015).

Reports described pVHL213 folding and aggregation *in vitro* (Shmueli et al., 2013; Sutovsky and Gazit, 2004). However, the aggregation propensity of the pVHL160 and pVHL172 isoforms has not been studied yet. As protein aggregation depends on macromolecular cytoplasm crowding, we overexpressed pVHL in fission yeast which does not require proteasome inhibition or stress to promote protein aggregation, differently from budding yeast. We found that pVHL proteins are incorporated in small dynamic aggregates and in large slow-moving inclusions. We then identified two pVHL mutations in ccRCC (P86L and P146A) that promote pVHL aggregation. P86L stimulated pVHL incorporation in small aggregates, while P146A exacerbated large inclusion formation. Conversely, the I151S mutation, which is located in the same aggregation-prone region as P146, reduced large inclusion formation and led to protein destabilization. Finally, we showed that the conserved gene *pac10* encoding a chaperone prefoldin subunit controlled pVHL stability.

Results

1. Human pVHL213 aggregates in fission yeast

In the absence of ELOB and C, pVHL213 aggregates in proteasome-deficient budding yeast cells (Kaganovich et al., 2008). To investigate the mechanism of pVHL aggregation in the fission yeast *Schizosaccharomyces pombe* in the absence of cofactors, yeast cells that express the Hsp104-GFP chaperone, a marker of damaged proteins (*hsp104-GFP* cells), were transformed with pREP1-VHL213 plasmid (Table S1) controlled by the thiamine-repressed strong *nmt1* promoter. Western blot analysis of cells cultured without thiamine for 24h confirmed the induction of pVHL213 expression (VHL213 ON, Fig. 1A) and showed that it was partially insoluble (VHL213 ON, lane P, Fig. 1A). Concomitantly with pVHL213, Hsp104-GFP expression level also was up-regulated and a higher amount was recovered in the pellet fraction (VHL213 ON, lane P, Fig. 1A), differently from control cells (empty vector and VHL213 OFF, Fig. 1A). Moreover, immunofluorescence analysis showed that

untagged pVHL213 colocalized with Hsp104-GFP in a large cytoplasmic structure (Fig. 1B). Colocalization with Hsp104 in inclusions was still observed in *hsp104-GFP* cells that express pVHL213 tagged with Red Fluorescent Protein (RFP-VHL, Table S1, Fig. S1). This indicated that fusion of pVHL213 with a fluorescent tag does not alter its aggregation propensity. RFP-VHL-positive inclusions always colocalized with Hsp104-GFP. Some Hsp104-GFP inclusions did however not colocalize with RFP-VHL, suggesting that RFP-VHL aggregates do not saturate protein quality control sites.

In exponentially growing *hsp104-GFP* cells (control), Hsp104-GFP was evenly expressed in the nucleus and was also localized in one or two dots per cell, close to the nucleus (Fig. 1C, arrowhead) or to the cell end (Fig. 1C, arrow). These dots were detected in 55.6% of cells (Table S2; 46.1±8.0% of cells with a single dot and 9.5±7.6% of cells with two dots) and likely corresponded to Protein Quality Control (PQC) inclusions where damaged proteins accumulate.

In *hsp104-GFP* cells that overexpressed untagged pVHL213, the percentage of cells with Hsp104-GFP dots increased to 72.8% (Fig. 1C, pVHL213 ON; Table S2, pVHL213) due to the strong increase (three times) in the proportion of cells with two dots (Table S2, n=76, 28.2±5.9% *vs* 9.5±7.6% in control cells). Upon repression of pVHL expression by addition of thiamine for eight hours (Fig. 1C, pVHL213 OFF; Table S2, pVHL213 OFF 8h), the percentage of cells with inclusions decreased to 46.3% and the fraction of cells with two dots to 5.5±5.1%, similar to control cells (Table S2, pREP1 OFF 8h: 9.2±6.5%). The mean size of Hsp104-GFP inclusions was 0.25±0.13 μm^2 in control cells (Table S2, pREP1 ON) and was increased in pVHL213-overexpressing cells (0.58±0.37 μm^2, Table S2, pVHL213 ON, Mann-Withney test, p-value<0.01). After repression of pVHL expression with thiamine for eight hours, the mean size decreased to 0.30±0.24 μm^2 in pVHL213-overexpressing cells (Table S2, pVHL213 OFF 8h), but was not different compared to control cells (0.28±0.20 μm^2, Table S2, pREP1 OFF 8h).

Our results show that pVHL213 expression promotes the increase of the number and size of Hsp104-GFP-positive inclusions, and pVHL likely incorporates into large Hsp104-positive PQC inclusions.

Overexpression of GFP-VHL213 promotes the formation of two distinct cytoplasmic inclusions. To further characterize the inclusions, wild type fission yeast cells were transformed with pREP41-GFP-VHL plasmids in which expression was controlled by the mild inducible *nmt41* promoter (Table S1). GFP-VHL isoforms expression was ascertained by western blot analysis (Fig. 2A for a schematic representation of the three pVHL isoforms, Fig. 2B).

After overnight expression induction, GFP-VHL213 was detected as small, highly dynamic puncta, referred to as "Small Dynamic Aggregates" or SDA that showed Brownian movements, (Fig. 2C, arrows and Movie 1). GFP-VHL213-positive SDA were detected in 20% of live cells.

GFP-VHL213 also formed large slow-moving cytoplasmic Aggregates or LSA, (Fig. 2C, arrowhead; Fig. 2D, arrow and arrowhead) that were not observed in cells transfected with the empty vector (see below). Like Hsp104-GFP dots, GFP-VHL213 LSA appeared as a single large spherical aggregate at the end of cells (cell end LSA, ceLSA) (arrow, Fig.2D) or close to the nucleus (juxtanuclear LSA, juLSA) (arrowhead, Fig. 2D). Overexpression of GFP-VHL213 in yeast cells that express Amo1-RFP (a nuclear envelope marker fused to RFP) indicated that juLSA were outside the nucleus (Fig. 2E). Analysis of 99 confocal microscopy sections showed that juLSA were close to but never within the nucleus outlined by Amo1-RFP. After overnight expression induction, juLSA and ceLSA-containing cells represented approximately 10% and 15% of all cells. Some cells (4%) contained both a ceLSA and a juLSA. This percentage was lower than the fraction of *hsp104-GFP* cells with dots, suggesting that Hsp104 inclusions incorporate GFP-VHL213 only above a threshold of expression. To quantify LSA sub-cellular localization, the cell surface was arbitrarily divided into 5 equal segments including (a) the nucleus, (b) the intermediate regions between the nucleus and the cell periphery and (c) the cell periphery (the most distal segments at the cell ends; Fig. 2F, schematic representation of a cell). This showed that pVH213 LSA were more frequently present in the intermediate areas than at the cell periphery (73% vs 25%, respectively, n=347; Fig. 2F). To distinguish new and old cell poles (the new cell pole is produced during the last cell division), cells were stained with the fluorescent cell wall marker aniline blue and LSA distribution was assessed relative to the two poles. GFP-VHL213-positive LSA were equally located at the new and old cell ends (48±8.3% versus 52±8.3%, respectively; n=126; see below).

It was previously shown that large inclusions of stress-induced misfolded proteins are the result of the fusion of small puncta. This fusion was shown to be reduced to 50% in the absence of the small Heat Shock Protein coded by the *hsp16* gene (Coelho et al., 2014). In budding yeast, Q body formation was shown to depend at least in part on the *hsp16*-homolog *HSP42* gene (Escusa-Toret et al., 2013). However, in fission yeast, we observed that both GFP-VHL213 SDA and LSA were detected in *hsp16Δ* cells (Fig. 2C) in identical proportion than in wild type cells, strongly suggesting that SDA are not counterparts of budding yeast Q bodies.

Disruption of the microtubule (MT) cytoskeleton with the MT-depolymerizing drug methyl benzimidazol-2-yl-carbamate (MBC) did not have any effect on LSA formation (38.4% of LSA-containing cells, n=429 *versus* 36.7%, n=452 for DMSO-treated cells) or localization, indicating that MT are not involved in LSA biogenesis and subcellular localization (Fig. S2A). Similarly, incubation

with Latrunculin B (LatB) to depolymerize the actin cytoskeleton did not significantly alter LSA formation (28.3% of LSA-containing cells, n=420 *versus* 33.9%, n=318 for DMSO-treated cells) or localization (Fig. S2B). Neither MBC nor LatB affected SDA dynamics consistent with previous results (Coelho et al., 2014).

The intracellular movements of ceLSA were mainly slow (Movie 2) and were probably driven only by the cytoplasmic flow and cytoplasmic constraints. The movements of juLSA were very limited, possibly due to a physical link with nucleus. LSA slow movements suggest that their localization may reflect the site of formation.

Finally, the aggregation propensity of a protein is mainly dependent on the proportion of hydrophobic residues in the primary sequence. We thus tested whether overexpression of two unrelated GFP-tagged proteins with a similar proportion of hydrophobic amino acids as pVHL213 (24.8%) would promote their aggregation in fission yeast cells. Overexpression of *Xenopus laevis* Cl2 (102 amino acids with 25.5% of hydrophobic residues) and of fission yeast Rad25 (270 amino acids with 23.4% of hydrophobic residues), driven by the *nmt41* inducible promoter (Table S1), did not give rise to detectable fluorescent aggregates (Fig. S3), supporting the hypothesis that pVHL aggregation is an intrinsic property promoted by a specific primary sequence.

Ubiquitination of GFP-VHL213 modestly participates in aggregate formation and may regulate the spatial distribution of misfolded pVHL. It has been shown that juxtanuclear inclusions contained only ubiquitinated proteins (Kaganovich et al., 2008), but this view has been recently challenged (Miller et al., 2015). In pVHL213, there are three lysine residues that could be subjected to ubiquitination, sumoylation and/or neddylation (Cai and Robertson, 2010; Cai et al., 2010; Park et al., 2015; Stickle et al., 2004). To determine whether pVHL ubiquitination may regulate its spatial distribution in cellular inclusions, we expressed a GFP-VHL213 variant in which these three lysine residues were mutated into arginine (K159R K171R K196R, hereafter referred to as 3KR, Fig. 2G, Table S1). Western blot analysis showed that wild type and 3KR GFP-VHL213 were similarly expressed with comparable proportions of insoluble and soluble pools (Fig. 2H). Likewise, the overall percentage of cells with wild type or 3KR GFP-VHL213 LSA was similar (approx. 30%). However, in 3KR-expressing cells, the proportion of ceLSA was higher than in cells expressing wild type GFP-VHL213 (Fig. 2G, t0). This result suggests that pVHL ubiquitination, neddylation and/or sumoylation may potentially influence its spatial distribution in different inclusions, although incorporation exclusively in a single inclusion type was not observed, differently from budding yeast (Kaganovich et al., 2008).

LSA contain immobile, terminally aggregated polypeptides. Monitoring GFP-VHL213 LSA formation dynamics over time indicated that LSA were assembled and disassembled in approximately 30 minutes in a hemicell (Fig. 3A and 3B, Movies 3 and 4). These observations suggest that LSA metabolism is limited in space. We then asked whether proteins incorporated into inclusions are terminally aggregated, insoluble products. After overnight expression induction, GFP-VHL213 expression was repressed with thiamine to prevent *de novo* LSA formation and protein mobility in LSA was monitored using the Fluorescence Recovery After Photobleaching (FRAP) method. After photobleaching of an area in the cytoplasm, cytoplasmic GFP-VHL213 diffused freely with fluorescence recovery in 30 seconds (Fig. 3C). Conversely, after photobleaching of an identical area corresponding to a whole GFP-VHL213 LSA (Fig. 3D), very limited fluorescence was recovered, indicating that bleached proteins within the LSA were immobile and could almost not be replaced by proteins from the cytoplasmic GFP-VHL213 pool. The observation that the fluorescence of a nearby unbleached LSA was unaffected by cytoplasm bleaching also strongly suggests that proteins could not diffuse from the cytoplasm into the inclusion (Fig. 3C). Finally, partial photobleaching of LSA did not result in fluorescence redistribution within the aggregate (Fig. 3E) as described in budding yeast (Kaganovich et al., 2008). We concluded that GFP-VHL proteins incorporated into large inclusions (LSA) were immobile and could be terminally aggregated products.

A balance between *de novo* pVHL aggregate formation and proteasome degradation. The *nmt41* promoter is fully repressed one hour after addition of thiamine in the medium. The expression of GFP-VHL213 was reduced in both the soluble and insoluble fractions, compared to induced cells, three and six hours after thiamine addition (Fig. 4A, OFF). Analysis of cells containing GFP-VHL213-positive LSA at three (t3) and six hours (t6) after addition of thiamine showed that juLSA had already disappeared at t3, whereas ceLSA progressively decreased over time (Fig. 4B). This indicates that the degradation rates of these structures are different and strongly suggests that the formation of juLSA and ceLSA correspond to two different protein quality control processes. Similar results were obtained also with 3KR GFP-VHL213, suggesting that ubiquitination does not influence the rate of aggregate clearance (Fig. 2G, OFF).

Aggregated proteins are cleared through two different pathways: autophagy and proteasome degradation. To identify the clearance pathway of pVHL inclusions, pVHL213 was expressed in *atg*1Δ cells, an autophagy-deficient fission yeast mutant (Mukaiyama et al., 2009). The formation of pVHL-positive aggregates (SDA and juLSA or ceLSA) and their clearance were unaffected in *atg*1Δ cells compared to wild type cells (Fig. 4C). Conversely, inclusions persisted longer in pVHL213-expressing cells incubated with the proteasome inhibitor bortezomib (BZ) than

with vehicle alone (DMSO, Fig. 4D and 4E), demonstrating that proteasome degradation is the main clearance pathway of pVHL inclusions. Strikingly, SDA formation was dramatically increased after one hour of BZ incubation (Fig. 4D and 4F), suggesting that these aggregates are extremely sensitive to proteasomal degradation. Consistently, the formation of SDA and LSA, including cells with two or more LSA (2+ LSA, Fig. 4G), was strongly promoted in *mts3-1* cells, a thermosensitive proteasome mutant.

2. Aggregation of pVHL172 and pVHL160 isoforms

The GFP-VHL172 isoform forms small dynamic aggregates and intermediate sized inclusions. In fission yeast cells that express GFP-VHL172 (Fig. 5A, white arrowhead), we detected only rare, small dynamic puncta reminiscent of pVHL213 SDA and inclusions of intermediate size compared to LSA (Fig. 5B). Consistently, overexpressed GFP-VHL172 was almost completely absent in the insoluble fraction (Fig. 5A, VHL172, P). This indicates that the main aggregation-prone region of pVHL lies within exon 2 (amino acids 114 to 154). GFP-VHL172-positive inclusions were still detected in the autophagy-deficient mutant. Consistently, untagged pVHL172 (pREP1-VHL172 plasmid, Table S1) colocalized with Hsp104-GFP, like pVHL213 (Fig. 5C). GFP-VHL172-positive inclusions were mainly located in the central region (Fig. 5D). We observed that soluble GFP-VHL172 occasionally accumulated in the nucleus, suggesting that the pVHL172 isoform has specific nuclear import signals or lacks nuclear export signals. Following protein expression repression, GFP-VHL172 aggregates were rapidly degraded. An aggregation-prone region is still present in the pVHL172 isoform because, as for GFP-VHL213, GFP-VHL172 formed SDA-like structures and intermediate inclusions and the number of SDA-like puncta was also strikingly increased after incubation with BZ (Fig. 5E).

The GFP-VHL160 isoform aggregates both into dense puncta and irregularly shaped large inclusions. GFP-VHL160 overexpressed in fission yeast cells (Fig. 5A, black arrowhead) was incorporated in highly dynamic, very dense small puncta (Fig. 5F, arrow) throughout the cytoplasm. These puncta were of more heterogeneous sizes and intensities compared to GFP-VHL213 SDA. GFP-VHL160 was also found in very large LSA-type inclusions (Fig. 5F, arrowhead, LSA; Movie 5). The shape of GFP-VHL160-positive LSA was irregular, differently from GFP-VHL213- and GFP-VHL172-positive inclusions that were round-shaped. Their formation started as early as nine hours after promoter de-repression. pVHL160 puncta formation was followed by the appearance of large and irregular LSA, although puncta-containing cells were still observed. These inclusions were never

located close to the nucleus. Most pVHL160-positive large aggregates (Fig. 5D, 70%, n=183) were in the cell periphery. Strikingly, almost all the GFP signals were present in aggregates suggesting that most of the GFP-VHL160 pool was insoluble. This was confirmed by the accumulation of GFP-VHL160 in the insoluble fraction (Fig. 5A, P). Interestingly, there was a strong bias towards accumulation of GFP-VHL160 LSA in the old cell pole in contrast to the situation with GFP-VHL213 LSA (Fig. 5G). These results suggest that inclusions subcellular localization may be regulated through different assembly site specifications and/or tethering mechanisms, the nature of which remains to be identified. The percentage of cells containing GFP-VHL160-positive LSA-type inclusions decreased after 18h, as observed for the two other pVHL isoforms, whereas small puncta persisted longer. However, the overall percentage of GFP-VHL160-expressing cells with aggregates -either small puncta or inclusion-did not decline (present in approximately 90% of yeast cells), contrary to other pVHL isoforms. This suggests that the threshold level for their formation is low and that their degradation might be slowed down compared to other pVHL aggregates. These observations suggest that GFP-VHL160 aggregates are strongly resistant and persist in cells, likely reflecting a higher propensity of GFP-VHL160 to aggregate compared to the other isoforms.

In contrast to pVHL213 and pVHL172, the pVHL160 isoform showed a distinct behavior if it was not GFP tagged. While expressing pVHL160 in the absence of the tag, we did not observe bigger Hsp104-GFP inclusions in cells nor Hsp104-GFP in the insoluble protein fraction. The untagged pVHL160 expressed protein was present in the soluble fraction (unpublished results). As the GFP fusion was the same for all pVHL isoforms, the different aggregation behavior of pVHL160 with or without a tag may be explained by a specific effect of the tag on the structural conformation.

In conclusion, pVHL172 has a low propensity to form aggregate, while pVHL160 aggregates in dense, dynamic SDA-type and large insoluble LSA-type structures.

3. pVHL tumorigenic mutations that are predicted to increase pVHL insolubility stimulate pVHL aggregation in fission yeast

To identify potential aggregation-prone regions (APR), using the TANGO algorithm (Fernandez-Escamilla et al., 2004), a highest pVHL aggregation propensity score corresponding to the hydrophobic stretch IFANIT within exon 2 (aa147-152, APR3; Fig. 6A) was revealed. Two other motifs with lower scores in TANGO were located within exon 1 (APR1 and APR2) and corresponded to aa72-78 (SQVIFCN) and aa87-91 (VWLNF), respectively (Fig. 6A). Then, the TANGO overall aggregation scores of VHL missense mutants identified in patients with ccRCC were calculated (Table S3). The scores were compared with two alternative algorithms (Conchillo-Sole et al., 2007; Tartaglia et al., 2008) and three mutations were selected: P86L, P146A and I151S (Fig. S4). The position of P86 and

P146 in the pVHL structure based on the 1LM8 dataset of PDB corresponding to pVHL160 (Fig. 6A, upper panel,) suggested that these residues were involved in the formation of β sheets essential for the structural organization of the exon1-exon2 linker region. Therefore, they could contribute to the tertiary structure of pVHL. In addition, the P86L mutation created a continuous hydrophobic stretch between APR1 and APR2, whereas the P146A mutation increased the TANGO score of APR3 by two-fold (Fig. S4). Finally, I151S was identified as an aggregation-suppressive mutation that completely abolished the aggregation propensity predicted in APR3 (Fig. S4). However, the I151 residue did not seem to be involved in the pVHL secondary structure, based on its position (Fig. 6A).

We tested the identified APRs and the potential impact of the selected ccRCC mutations, by overexpressing pVHL213 mutants in our fission yeast inducible system. Western blot analysis showed equivalent expression levels for GFP-VHL213 P86L and P146A compared to wild type GFP-VHL213, whereas the expression of the I151S was moderately reduced (Fig. 6B).

The P86L mutation promotes the formation of SDA, the P146A mutation increases the size of LSA while I151S has the opposite effect. The number of cells containing SDA was increased in cells expressing GFP-VHL213 P86L compared to wild type GFP-VHL213-expressing cells (Fig. 6C, 41.9% vs 16.9%). Conversely, the number of LSA was not different, suggesting that the P86L mutation affected only the formation of SDA. After fixation, no SDA-containing cell was detected in wild type GFP-VHL213-expressing cells whereas SDA were still observed in some GFP-VHL213 P86L-expressing cells (Fig. 6C, lower panels). Consistent with the higher aggregation propensity score of APR3 harboring the P146A mutation (Fig. S4), larger LSA were observed in cells expressing GFP-VHL213 P146A than in cells expressing wild type GFP-VHL213 (Fig. 6D; mean sizes: 0.595±0.33 μm^2, n=254 *vs* 0.543±0.38 μm^2, n=294, respectively; Fig. 6E, Mann-Withney test, p-value=0.005). The fraction of cells with LSA was not significantly changed, suggesting that the maximal number of cells containing pVHL inclusions was reached in our experimental conditions. Interestingly, the proportion of cells with LSA was lower in GFP-VHL213 I151S- than for wild type GFP-VHL213-expressing cells and LSA appeared smaller (Fig. 6D and 6E, mean size: 0.441±0.24 μm^2, n=182, although not significantly different from the WT, Mann-Withney test, p-value=0.09).

4. The prefoldin subunit Pac10 is required for pVHL aggregate formation

The conserved multi-protein chaperone complex prefoldin composed of six different subunits (two alpha and four beta subunits; PFDN1-6 in humans) that are organized in a double-barrel structure is involved in protein folding and aggregation of misfolded proteins. The prefoldin subunit PFDN3 (or VBP-1 for VHL Binding Protein 1) is a direct pVHL binding partner in human cells (Tsuchiya et al.,

1996) and Pac10 is the VBP-1 homolog in fission yeast. To investigate the potential role of the prefoldin subunit in pVHL folding, GFP-VHL isoforms were overexpressed in a *pac10* deletion mutant. Compared to wild type cells, *pac10Δ* cells showed a strong reduction in GFP-VHL expression (Fig. 7A). Moreover, formation of GFP-VHL213-positive inclusions was dramatically reduced in *pac10*-deleted cells (Fig. 7B, left panel; 6.5±4.5%, n=757, and 32.4±12.3%, n=610, of LSA containing cells in *pac10Δ* and WT, respectively). This indicated that Pac10 contributed to their formation. However, GFP-VHL213- and GFP-VHL160-positive small aggregates were still detected in *pac10Δ* cells, strongly suggesting that small puncta/SDA were Pac10-independent structures. In *pac10Δ* cells, the GFP-VHL213 P146A mutant could form significantly more LSA than wild type GFP-VHL213 (Fig. 7B, right panel, 19.5±1.6% vs 6.5±4.5%, respectively) even though expression levels were similar (Fig. 7A), suggesting that the aggregation-prone P146A mutation bypassed the requirement of Pac10 for pVHL aggregation. Specifically, Pac10 regulated pVHL stability and *pac10* deletion could maintain wild type pVHL expression below the threshold required for large aggregate formation. However, the aggregation-prone P146A mutation might lower this threshold, allowing the formation of LSA also in *pac10Δ* cells.

Discussion

Misfolded pVHL forms aggregate *in vitro* (Shmueli et al., 2013; Sutovsky and Gazit, 2004) in yeast cells (Escusa-Toret et al., 2013; Kaganovich et al., 2008; Miller et al., 2015; Specht et al., 2011; Spokoini et al., 2012) and also in mammalian cells (Ogrodnik et al., 2014; Weisberg et al., 2012). In cancer cells, protein quality control mechanisms are increasingly altered with the pathology severity. Therefore, proteins with a high susceptibility to unfold, such as pVHL, might be more destabilized in tumor cells. Furthermore, misfolded proteins could also co-aggregate normal native partner proteins that consequently cannot carry out their functions (Olzscha et al., 2011). Moreover, some VHL missense mutations do not alter directly pVHL function, but affects protein stability leading to loss of function. Targeting pVHL stabilization is of potential therapeutic value (Ding et al., 2014; Yang et al., 2013). Thus we investigated potential aggregation-prone pVHL mutations and pVHL aggregation dynamics in fission yeast. We show that pVHL can aggregate in two forms: small dynamic aggregates (SDA) and large inclusions (LSA) and this is at least due to two distinct parts of the protein (see model Fig. 8). Furthermore pVHL mutations found in patients with ccRCC promote distinct pVHL aggregation patterns.

Expression of heterologous aggregation-prone proteins has been widely studied in yeast models. We set up a new easy assay to monitor pVHL aggregation in which MG132 and heat stress are not required to promote aggregation like in budding yeast. In contrast to a recent report in

budding yeast (Brock et al., 2015), we did not observe any impact of the putative fission yeast Elongin C homolog on pVHL213 stability (data not shown).

Our data are consistent with size exclusion chromatography using recombinant pVHL213 protein that showed the existence of aggregates of different sizes (Shmueli et al., 2013). SDA may correspond to a local aggregation of co-translationally produced polypeptides at a small distance range. We hypothesize that they form immediately after ribosome exit in cells with overwhelmed protein quality control mechanisms due to excessive protein expression. SDA are highly proteasome-sensitive and thus they are only very transiently detected. These structures are formed by an aggregation mechanism involving the NH_2-terminal aggregation-prone regions (APR1 and APR2) in exon 1 that are first exposed to the cytoplasm during protein synthesis. Furthermore, pVHL-positive SDA formation does not require stress conditions nor Hsp104 and might thus only depend on the intrinsic properties of the pVHL primary sequence. We propose that these structures self-assemble because we observed them in all situations, including in *hsp16Δ* and *pac10Δ* cells, where the formation of large aggregates is inhibited. SDA resembled stress-induced Q bodies described in budding yeast (Escusa-Toret et al., 2013). In fission yeast, SDA were not observed in *hsp104-GFP* or *hsp104-mCherry* (unpublished results) cells overexpressing pVHL213, indicating that they correspond to Hsp104-free aggregates. Fusion of stress-induced aggregates was reduced to 50% in *hsp16Δ* cells (Coelho et al., 2014). We found that the proportion of GFP-VHL213 SDA and LSA containing cells was indistinguishable between wild type and *hsp16Δ* cell populations, strongly suggesting that LSA are not the result of an Hsp16-dependent fusion of SDA. Thus we considered that, in fission yeast, SDA and LSA corresponded to two structurally unrelated pVHL-containing inclusions that formed independently. We observed that wild type GFP-VHL213 and GFP-VHL172 disappeared after formaldehyde fixation but not GFP-VHL213 P86L or GFP-VHL160, suggesting that there may be several populations of small aggregates with distinct structural properties.

Even under normal growth condition, fission yeast cells exhibited Hsp104-positive dots like in budding yeast (Saarikangas and Barral, 2015). Upon pVHL overexpression, large Hsp104-positive pVHL inclusions were located either at the cell ends or close to, but clearly outside the nucleus in contrast with the recent observations in budding yeast (Miller et al., 2015). Spokoini *et al.* reported a link between the IPOD and the large vacuole of budding yeast (Spokoini et al., 2012). However, fission yeast contains approximately eighty small vacuoles that are homogeneously distributed in the cytoplasm. Therefore, in fission yeast, the mechanisms determining the site of ceLSA formation remain to be elucidated.

The disruption of MT or F-actin did not impact the LSA or SDA localization and dynamics, suggesting cytoskeletal-independent behaviors. Similarly, both the MT and F-actin networks are not

involved in stress-induced aggregate formation in fission yeast (Coelho et al., 2014). Moreover, there was no biased localization of pVHL213 LSA towards one cell pole, suggesting that LSA localization may be independent of new cell pole establishment.

Using *in silico* methods we identified three potential APR in pVHL. In yeast, both pVHL160 and pVHL213 form large inclusions, whereas pVHL172, which lacks APR3, only rarely form inclusions and of small size. This suggests that APR3 is critical for the formation of large pVHL inclusions. Indeed, pVHL mutations located within or close to APR3 affected its aggregation. The P146A mutation increases the aggregation score of APR3 and this mutant formed larger inclusions than the wild type pVHL. Conversely, the I151S mutation lowers the aggregation score of APR3 and seems to decrease the inclusion size, suggesting a correlation between the APR3 aggregation score and the size of inclusions in cells.

The APR1 and APR2 regions are present in all three pVHL isoforms. As all pVHL isoforms formed SDA, we hypothesize that APR1 and APR2 are involved in SDA formation. In agreement, the P86L mutation strongly enhances APR1-APR2 aggregation score by bridging these two regions in a single long hydrophobic stretch and we consistently observed a higher proportion of SDA in the pVHL P86L-expressing cells.

APR3 lies in the β strand region of exon 2 whereas APR1 and APR2 are in the NH_2-terminal part of pVHL. The folding of the APR3 region may be slower than the NH_2-terminal part and may require distinct chaperones and mechanisms. Our structural analysis of pVHL (Fig. 6A) suggests that the P86L mutation would not disrupt, but only disturb the interaction between the β sheets 3 and 7. In contrast, the P146A mutation would disrupt the interaction between the β sheets 8 and 9 and the β sheet 2, leading to an incomplete terminal folding of the pVHL protein. These distinct structural effects of the mutations may explain the formation of different types of aggregates.

The chaperonin TRiC binds to the exon 2 region of VHL and is involved in pVHL213 folding (Feldman et al., 1999). This essential protein complex is conserved in fission yeast and thus may influence pVHL213 aggregation. However, Feldman *et al.* (2003) reported that alanine substitutions in amino acids 144-147 of pVHL did not alter TRiC binding, whereas that I151S mutation reduced the binding efficiency of pVHL to TRiC (Feldman et al., 2003). Thus, the effect of the P146A mutation on aggregation may not involve TRiC interaction. Conversely, the reduced TRiC binding to pVHL I151S may contribute to the lower stability of this mutant in cells. Defining the exact contribution of TRiC in this process would require conditional mutant alleles.

Ubiquitination on Lys171 and Lys196 residues was reported in mammalian cells (Cai and Robertson, 2010; Park et al., 2015). Park *et al.* recently showed that 3KR mutant was not ubiquitinated in contrast to wild type pVHL213 (Park et al., 2015). These residues are highly

conserved in different species, suggesting that ubiquitination might also be conserved. After verifying that the aggregation score of the 3KR mutant was indistinguishable from that of the wild type protein, we investigated the aggregation of a triple 3KR mutant. The 3KR mutation has no effect on pVHL stability and the percentage of LSA-containing cells was unchanged. Ubiquitination did not control a specific subcellular localization of pVHL aggregates, but we detected an increase in ceLSA over juLSA formation in the 3KR mutant, suggesting that fine-tuned targeting mechanisms may operate to sort aggregate proteins into ceLSA and juLSA.

The prefoldin complex acts in mediating protein folding by targeting substrate proteins to the chaperonin TRiC. Here, we found that in the absence of Pac10 (the VBP-1 fission yeast homolog), pVHL can still form SDA, but not LSA. This suggests that Pac10 plays a role in the incorporation of misfolded pVHL into large inclusions, possibly through direct interaction with pVHL as in human cells (Tsuchiya et al., 1996). Moreover, pVHL protein level was reduced in *pac10Δ* cells, suggesting that Pac10 interaction contributes to pVHL stability. In its absence, misfolded pVHL may be rapidly degraded because SDA are proteasome-sensitive. We hypothesize that pVHL binds transiently to Pac10 prior to folding and this step may be critical to prevent its rapid degradation. The observation that pVHL P146A, but not P86L or I151S, has a higher propensity to form aggregates suggests that this mutation bypasses the protective effect of Pac10. It will be of interest to study the impact of modulating the expression of the prefoldin subunit VBP-1 on the half-life of endogenous pVHL in mammalian cells. Characterization of the prefoldin-mediated folding pathway for VHL should prove important for a better understanding the VHL disease and for the identification of new pharmacological targets.

It has been shown that VHL mRNA levels were unaffected in some VHL-related pathologies despite pVHL loss-of-function (Yang et al., 2013). These observations were sometimes correlated to an increased rate of mutated pVHL protein degradation. This rate may vary depending on the mutation and/or the protein quality control efficiency of cells. Thus the exact impact on the VHL loss of function mediated disease remains difficult to predict. This notion supports a better understanding of mechanistic principles of pVHL folding and an in-depth characterization of missense pVHL mutations affecting them. Here we show that some pVHL mutations can result in the incorporation of pVHL213 into insoluble aggregates. Aggregation of pVHL213 into many small or a large aggregate has the same effect as degradation, which is to lower the cytoplasmic fraction available to perform its tumor suppressor function.

Materials and Methods

S. pombe strains, media and reagents

S. pombe strains used in this study were listed in Table S4. Media and genetic methods were as described (Moreno et al., 1991). Cells were grown at 30°C. Thiamine (Sigma) was added to a final concentration of 2 μM. For non-standard growth conditions, cells were grown in 1 mM Bortezomib (ApexBio), 20 μM LatB (Calbiochem), 25 mg/ml MBC (Sigma) or DMSO (Sigma).

Molecular cloning

Plasmids used in this study are listed in Table S1. The pCMV-hVHL213 (a kind gift from Dr A. Buchberger, Würzburg, Germany), which contains human VHL ORF cDNA (amino-acids 1-213) was used as template for PCR-amplification with the VHL1S and VHL3AS primers (pVHL213), or with the VHL2S and VHL3AS primers (pVHL160) (Table S5). The amplicons were subcloned in the pGEM-T vector (Promega), or directly digested with the appropriate restriction enzymes (*Nde*I and *Bam*HI; New England Biolabs) for ligation in pREP1 or pREP41GFP. The pREP41-VHL172 and pREP41GFP-VHL172 plasmids were obtained after PCR amplification of the pVHL172 ORF (aa1-113+155-213 of pVHL213) from the IMAGE cDNA clone (Genbank BC058831) with VHL1S and VHL3AS. To generate RFP-VHL fusion construct, a 650-bp fragment was amplified (VHL11SalIS and VHL13SmaIAS primers). This *Sal*I-*Sma*I-digested PCR fragment was cloned into pSLF279 (generously provided by K.S. Chung, KRIBB, Korea). Point mutations (P86L, P146A, I151S or K159R/K171R/K196R) were introduced in the pVHL213 cDNA inserted in pREP41GFP, using a sequential two-step PCR approach (Table S5). All constructs were confirmed by Sanger sequencing and transformed in the appropriate yeast strains by the lithium/acetate method.

Western blotting

Cell cultures (50 ml) were harvested by centrifugation at 3,000 rpm at 20°C for 2 min, washed in 5 ml ice-cold STOP buffer (10 mM EDTA, 150 mM NaCl, 50 mM NaF, 0.05% NaN$_3$). Dried cell pellets were stored at -70°C. Cell pellets were lysed in lysis buffer (30 mM HEPES, pH 8.0, 150 mM NaCl, 1% glycerol, 1 mM DTT, 0.5% Triton, "Cocktail Set IV" Calbiochem protease inhibitor) with 425-600μm glass beads (Sigma) in a precellys24 homogenizer (Bertin) at 6100 rpm for 15sec thrice and clarified by centrifugation at 6,000*g* at 4°C for 5 min. Supernatants were divided in 40 μl aliquots. One aliquot was used as total protein; another aliquot was spun at 16,000*g* at 4°C for 30 min and designated as the soluble fraction (according to (Kaganovich et al., 2008)). Pellets were resolubilized by heating in

50 µl 1x SDS sample buffer. Ten µl of 5x SDS sample buffer was added to the total protein and soluble fraction samples. Equal amounts of each fraction were resolved by SDS–PAGE and transferred onto PVDF Immobilon-P membranes. Membranes were blotted in TBS/5% milk/0.05% Tween 20. Anti-VHL (Chesnel et al., 2015) and anti-GFP (11 814 460 001, Roche) antibodies were used at 1:1000 and 1:4000 dilution, respectively. As loading control, the mouse monoclonal anti-PSTAIR antibody (anti-Cdc2, P7962 Sigma) was used at 1:5000. Secondary antibodies were conjugated to alkaline phosphatase or horseradish peroxidase and revealed with ECF (GE Healthcare) or West DURA (Pierce), respectively.

Microscopy techniques

For time-lapse video microscopy, 2 µl of exponentially growing cells were mounted on 2% EMM agarose pads and images were captured at 30°C. GFP and mCherry/RFP signals were captured using spinning disk Nikon TE2000, Leica DMRXA, Leica DMIRB or confocal LEICA DMI 6000 CS microscopes. Nuclei were stained with 200 ng/ml DAPI (Sigma). For cell wall detection, cells were fixed with 4% formaldehyde (Sigma) for 30 min, washed in PBS followed by staining with 2.5µg/ml A488-conjugated isolectin (I21411, Molecular Probes). Images were acquired with the Metamorph software. Aggregate sizes were estimated from the area measured using the ImageJ software. FRAP data were acquired using a spinning disk Nikon TE2000 microscope and the Metamorph software: GFP signals were recorded every second during 3 min., the bleach was applied for 0.5 sec after 10 seconds. Normalized FRAP data were calculated with the ImageJ software. For indirect immunofluorescence experiments, cells were fixed with 4% formaldehyde and processed as described (Balasubramanian et al., 1997). Anti-VHL antibody (Chesnel et al., 2015) and Texas-red conjugated anti-mouse IgG antibodies (Molecular Probes) were used at 1/50 and 1/200, respectively.

Acknowledgments

Competing interests

No competing interests declared.

Author contributions

Conceived and designed the experiments: XLG FC YAB. Performed the experiments XLG FC AC CLG. Analyzed the data XLG FC YAB AC CLG CV. Contributed reagents/materials/analysis tools: OD (molecular modelling), SD (sequencing) Wrote the paper XLG
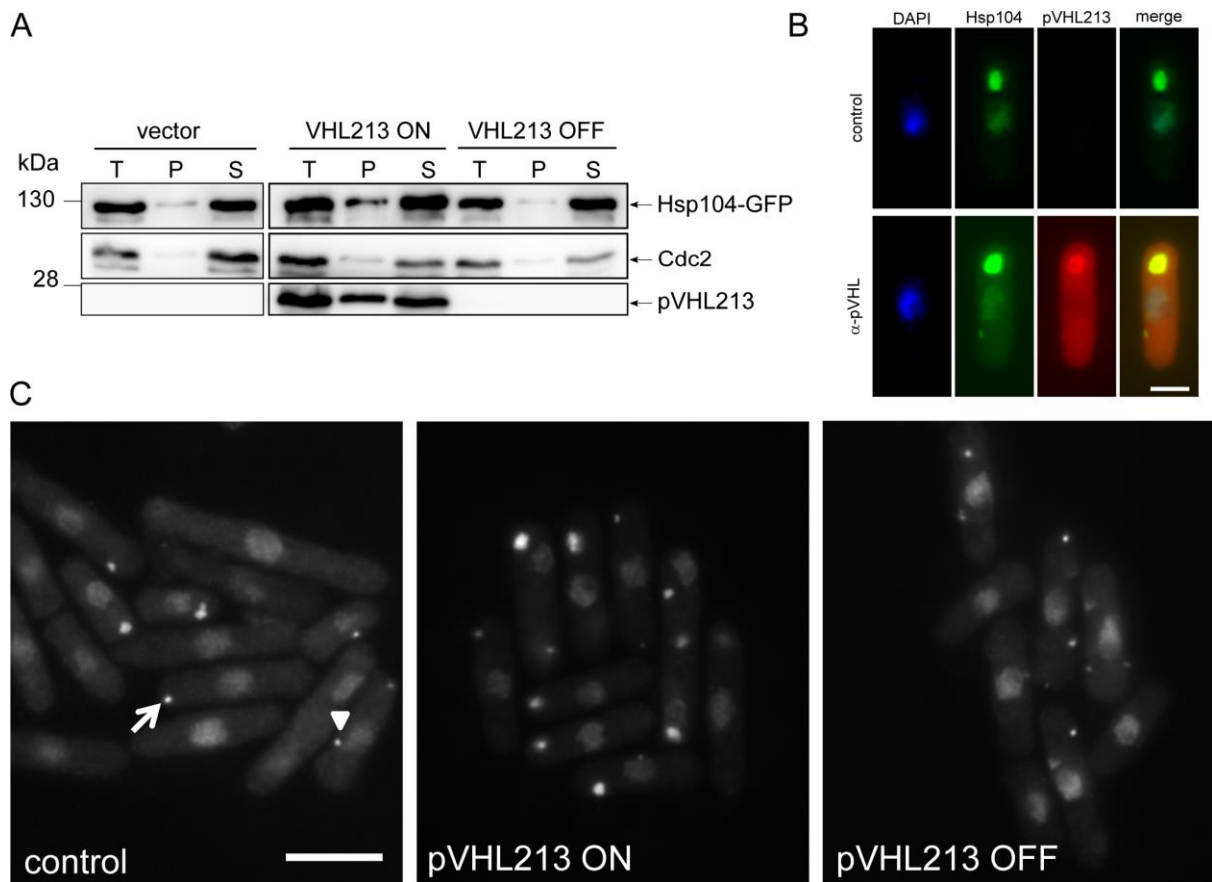
Fundings

Figures

Figure 1: Human pVHL is incorporated in Protein Quality Control inclusions in fission yeast. (A) Western blot analysis of pVHL213 overexpression in *hsp104-GFP* cells: total cell lysates (T) and the soluble fraction (S) and insoluble fraction (P) were probed for expression of Hsp104-GFP (upper panel), pVHL (lower panel) and Cdc2, as control for the soluble fraction (middle panel). *Hsp104-GFP* cells transformed with the pREP1-VHL213 plasmid were cultured overnight without thiamine to induce pVHL213 expression (ON) or with thiamine to repress pVHL213 expression (OFF). Control cells (transformed with empty vector) were cultured in the ON condition. (B) Overexpressed untagged pVHL213 colocalizes with the Hsp104-GFP chaperone in a large cytoplasmic inclusion. Cells were processed for immunofluorescence using the anti-VHL 6030 antibody and stained with DAPI. Merge shows the superposition of fluorescent signals. Bar: 5 μm. (C) *Hsp104-GFP* cells were transformed with the pREP1 empty vector (control; left panel) or with the pREP1-VHL213 plasmid (middle and right panels). Protein expression was induced for 16h (ON) and then repressed for 8h (OFF). The arrow depicts an Hsp104-GFP dot in the distal part of the cell; the arrowhead shows a juxtanuclear Hsp104-GFP dot. Bar: 10 μm.
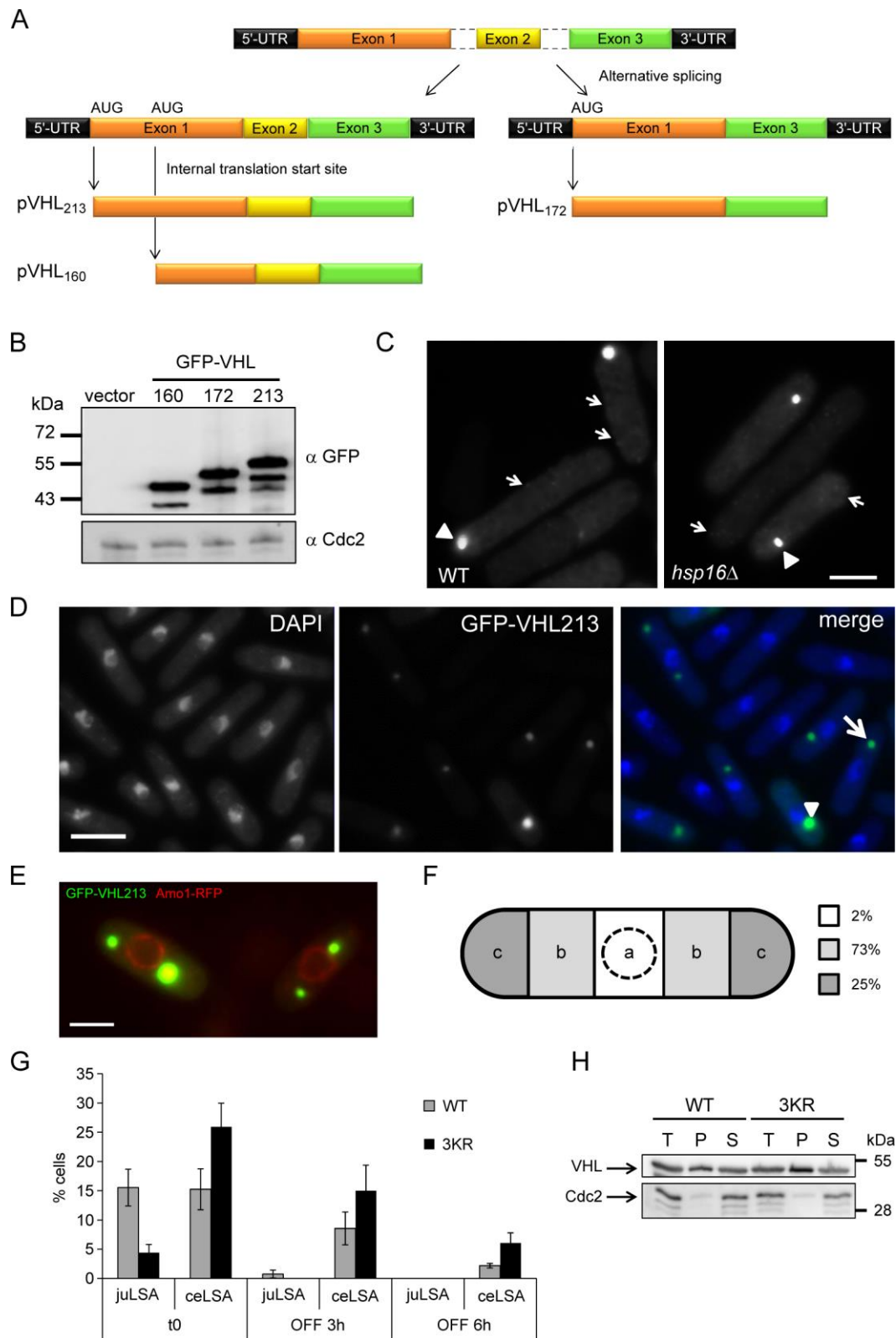
Figure 2: GFP-VHL213 forms two distinct aggregates. (A) Schematic representation of pVHL isoforms produced from the human *vhl* gene. (B) Western blot analysis of the expression of the three GFP-tagged pVHL isoforms after 16h induction. Vector, cells transformed with empty vector (control). Cdc2 expression was used as a loading control. (C) In wild type (left panel) and *hsp16Δ* (right panel)

live cells, GFP-VHL213 forms small cytoplasmic puncta (SDA) and large inclusions (LSA) indicated by arrows and an arrowheads, respectively. Bar: 5 μm. (D) GFP-VHL213 can also form one or two large spherical inclusions (LSA) either close to the DAPI-stained nucleus (arrowhead, juLSA), or towards the cell ends (arrow, ceLSA). Left panel: DAPI staining; middle panel: GFP-positive inclusions; right panel: merged fluorescent signals. Bar: 10 μm. (E) Merged image of *amo1-RFP* cells that express GFP-VHL213. Amo1 is a nuclear envelope marker. (F) Subcellular localization of GFP-VHL213 LSA. GFP-VHL213 overexpressing cells (n=347) were divided into five segments of the same size and the percentage of cells with LSA in the different segments was calculated. The nucleus is indicated by a dashed circle in the schematic representation of the cell. (G) Percentage of cells with a juLSA or a ceLSA in cells transformed with plasmids expressing wild type (WT) or the 3KR (3KR) mutant of GFP-VHL213. Cells were cultured in the ON condition for 16h (t0) and then in the OFF condition for 3h and 6h. Mean of three independent cultures. (H) Western blot analysis of the expression of the wild type (WT) and 3KR GFP-tagged pVHL versions after 16h induction: total cell lysates (T) and the soluble fraction (S) and insoluble fraction (P) were probed for expression of GFP-VHL (upper panel), and Cdc2 (lower panel), as control for the soluble fraction.
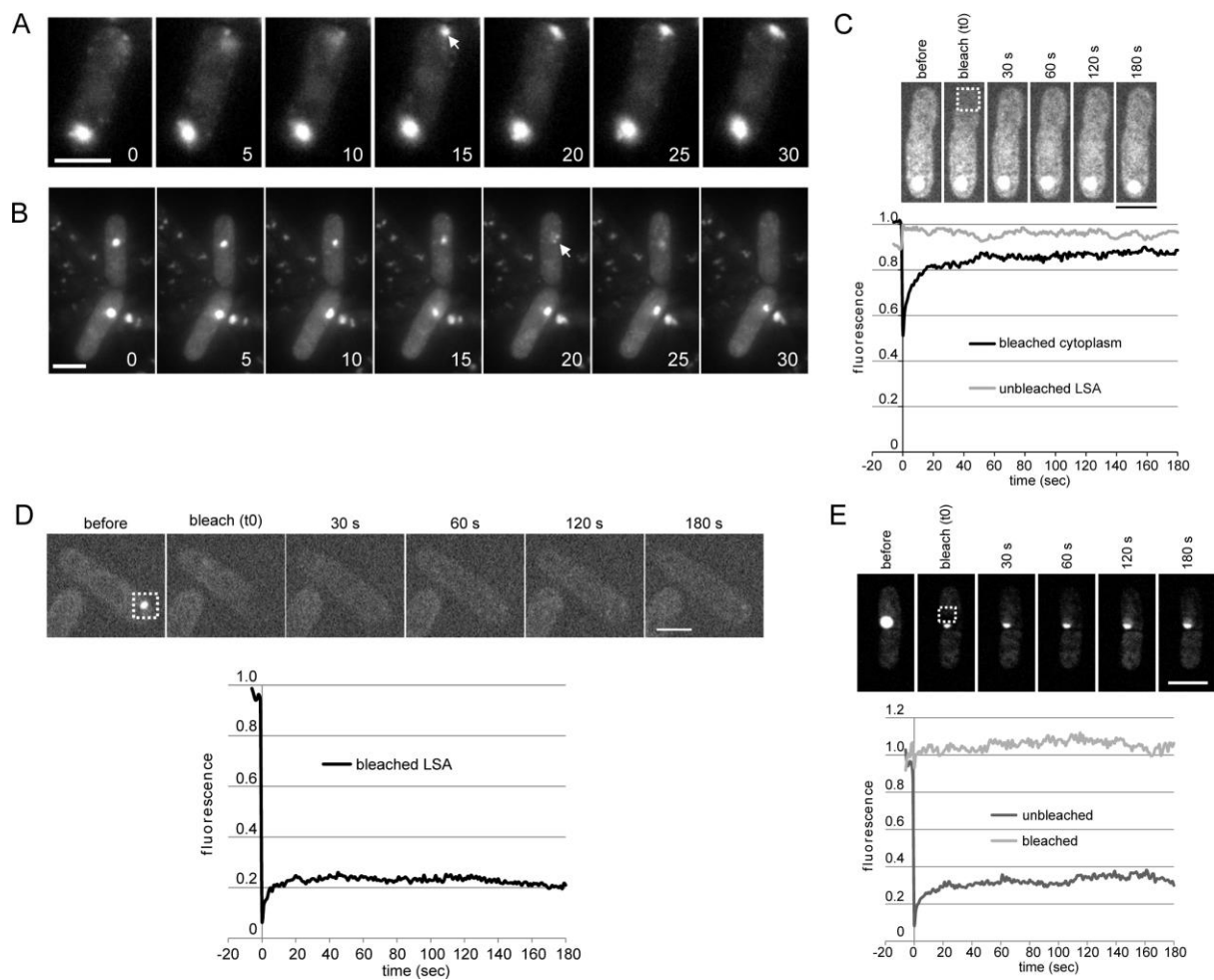
Figure 3: Dynamics of GFP-VHL pools within cells revealed limited exchanges between the cytoplasm and LSA. (A) Two LSA are present in the cell and one is formed *de novo* in the top of the cell (time is indicated in min.). (B) Two cells each with one LSA showed disappearance of LSA: in 30 min. (upper cell) or 50 min. (lower cell). (C), (D) and (E) Fluorescence Recovery After Photobleaching (FRAP) experiments. In C, the upper panel shows an example of laser photobleaching of an area (dashed square) within the cytoplasm of a cell that overexpresses GFP-VHL213 to monitor the mobility of the cytoplasmic pool of pVHL (bleached cytoplasm). One image of the cell was taken every second from seven seconds before the bleach up to 180 seconds after the bleach. The bottom curve shows the fluorescence recovery (mean curve of n=12 bleach experiments), the light grey curve shows the fluorescence recovery of an equally sized region of an unbleached LSA in the same cell. (D) FRAP experiment of a GFP-VHL213-positive LSA (dashed square). One image of the cell was taken every second from seven seconds before the bleach up to 180 seconds after the bleach (fluorescence recovery curve is the mean of n=15 LSA). (E) FRAP experiment applied to part of a GFP-VHL213-positive LSA (dashed square). Bleaching was applied to a limited sector of a LSA and

fluorescence recovery was monitored either in the bleached part or in the unbleached part of the LSA. One image of the cell was taken every second from seven seconds before the bleach up to 180 seconds after the bleach (fluorescence recovery curve is the mean of n=4 LSA). Bars: 5 μm.
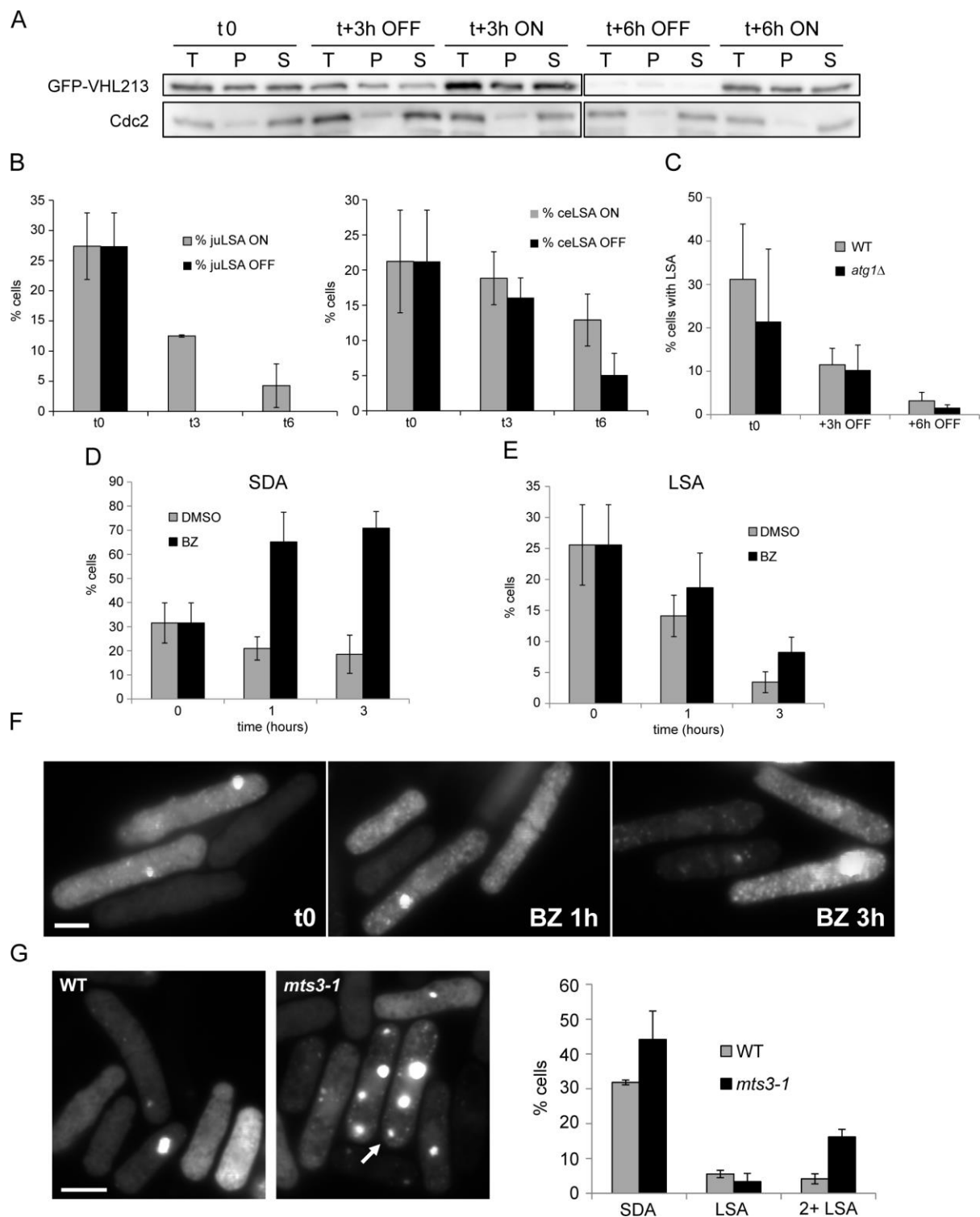
Figure 4: Aggregates are mainly cleared in a proteasome-dependent manner after repression of pVHL protein expression. (A) Western blot analysis of GFP-VHL13 expression in the pellet (P, insoluble) and supernatant (S, soluble) fractions of protein lysates after 16h of induction (t0) and then three and six hours later (+3h, +6h) in the absence (ON) or in the presence (OFF) of thiamine. (B) Percentage of cells with juLSA (upper panel) or ceLSA (lower panel) was calculated after 16h of

induction (t0) and after 3 hours (t3) and 6 hours (t6) without (ON) or with (OFF) thiamine. (C) GFP-VHL213-positive LSA clearance was compared in wild type (WT) and autophagy-deficient *atg1Δ* cells after expression repression (OFF) for 3h and 6h (mean of three independent experiments). (D-E) Protein expression was induced for 16h and then the percentage of cells containing pVHL213 SDA (D) or LSA (E) was scored 1h after addition of thiamine (t0) and then after incubation with 1 mM of the proteasome inhibitor bortezomib (BZ) for 1h and 3h. DMSO was used as control (mean of three independent experiments). (F) The panels show cells at t0 and after incubation with BZ for 1h and 3h. (G) Wild type (WT) and *mts3-1* proteasome mutant cells overexpressing GFP-VHL213 were scored after 6 hours at 37°C. Arrow indicates cells containing two or more LSA and/or numerous dense puncta (2+ LSA cells). The histogram on the right shows the percentage of cells containing SDA, one LSA or 2+ LSA (n=543 and n=738 cells for WT and *mts3-1*, respectively; mean of three independent experiments). Bars: 5 μm.
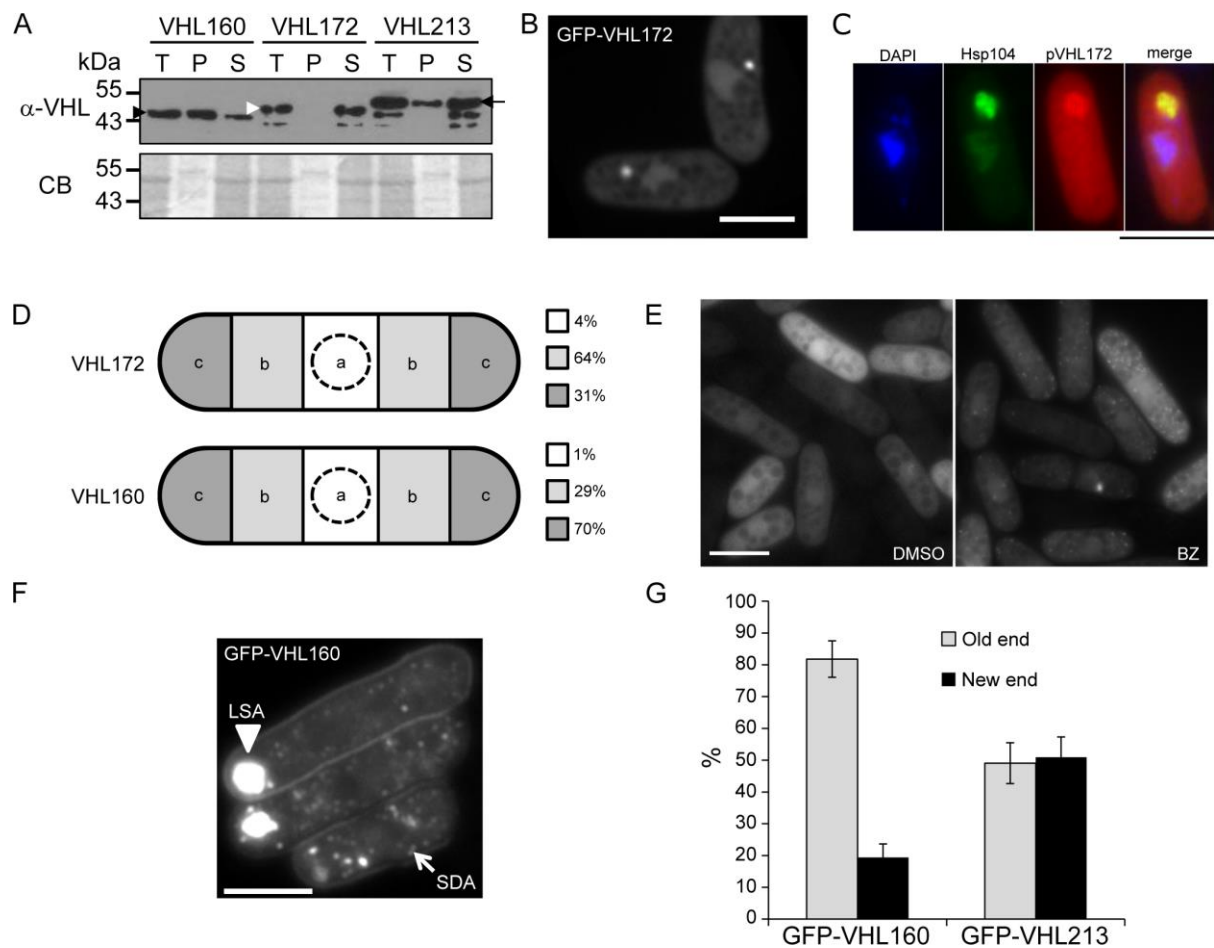
Figure 5: Overexpression of the GFP-VHL172 and GFP-VHL160 isoforms promotes distinct aggregate formation. (A) Western blot analysis of the expression of the different GFP-tagged pVHL isoforms (GFP-VHL160, black arrowhead, GFP-VHL172, white arrowhead, GFP-VHL213, black arrow;) after 16h induction: total cell lysates (T) and the soluble fraction (S) and insoluble fraction (P) were probed for expression of GFP-VHL (upper panel), and the gel was stained with Coomassie blue (CB, lower panel), as a loading control. (B) Cells overexpressing GFP-VHL172 formed small rounded inclusions. (C) Overexpressed untagged pVHL172 colocalizes with the Hsp104-GFP chaperone in a large cytoplasmic inclusion. Cells were processed for immunofluorescence using the anti-VHL 6030 antibody and stained with DAPI. Merge shows the superposition of fluorescent signals. (D) Subcellular localization of GFP-VHL160 and GFP-VHL172 LSA. GFP-VHL160 and GFP-VHL172 overexpressing cells (n=183 and n=74, respectively) were divided into five segments of the same size and the percentage of cells with large inclusions in the different segments was calculated. The nucleus is indicated by a dashed circle in the schematic representation of the cell. (E) The panels show cells overexpressing GFP-VHL172 after incubation with BZ or DMSO (control) for 3h. (F) Cells overexpressing GFP-VHL160 formed small, very dense puncta (arrow) and large irregular structures (arrowhead). (G) The percentage of distal LSA in the old *vs* the new cell ends was compared for GFP-

VHL160 and GFP-VHL213 (n=418 and n=126, respectively) using aniline blue co-staining to identify the cell poles. Bars: 5 μm.
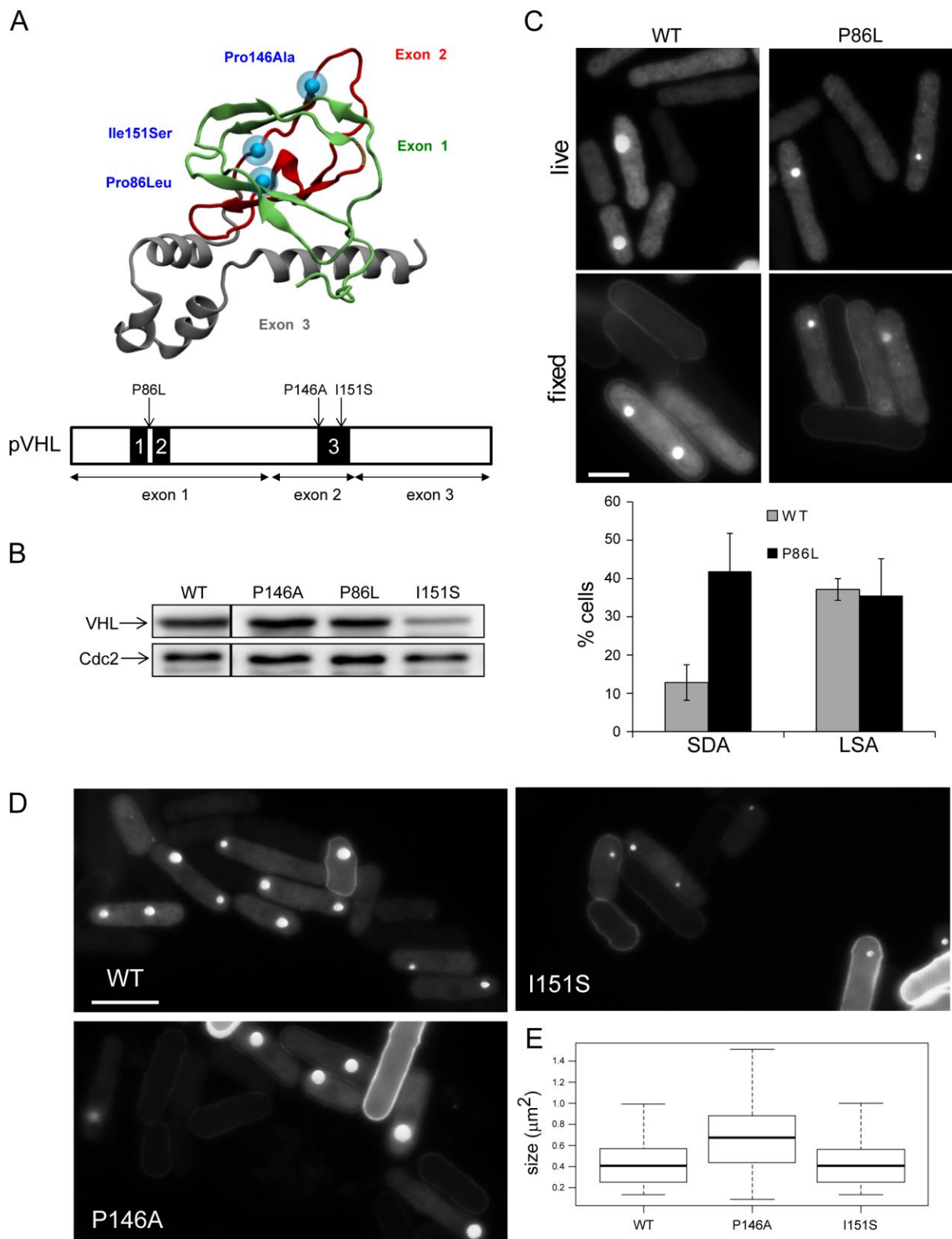
Figure 6: Distinct aggregation patterns of pVHL tumorigenic mutants. (A) Upper panel: Schematic representation of the pVHL structure. Exons and the corresponding protein domains are identified by a color code (green: exon 1; red: exon 2; grey: exon 3) and pVHL mutated residues are indicated in blue. Lower panel: Identification of Aggregation-Prone Regions (APR, black boxes) in pVHL primary

sequence using the TANGO algorithm. The positions of the mutated residues (P86L, P146A and I151S) and of the three exons are indicated. (B) Western blot analysis of the expression of wild type GFP-VHL213 (WT) and of the GFP-VHL213 P146A, I151S and P86L mutants using an anti-GFP antibody. Cdc2 was used as loading control. (C) Cells in which expression of GFP-VHL213 WT or P86L was induced for 16h were imaged live (upper panels) or after formaldehyde fixation (fixed, lower panels). Bar: 5 μm. The percentage of live cells with SDA and LSA is shown on the bottom histogram (mean of three independent cultures). (D) Cells in which expression of GFP-VHL213 WT, P146A or I151S was induced for 16h were imaged. Bar: 10 μm. (E) Mean size (surface area in μm^2) of LSA in cells in which expression of GFP-VHL213 WT (n=294), P146A (n=164) or I151S (n=182) mutants was induced for 16h.

Figure 7: The prefoldin subunit Pac10 is required for formation of large pVHL inclusions. (A) Western blot analysis of wild type (WT) and GFP-VHL213 P146A expression proteins in WT or *pac10Δ* cells after 16h induction. Cdc2 was used as loading control. (B) *Pac10Δ* cells after induction of WT or GFP-VHL213 P146A for 16h. Bar: 5 μm. (C) Percentage of cells containing pVHL213 LSA in each condition (mean of three independent cultures).

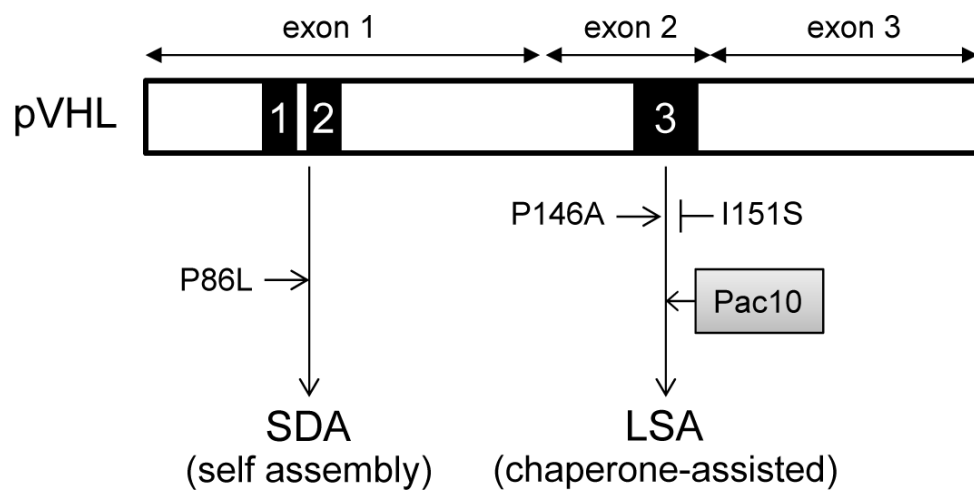**Figure 8: Model of pVHL aggregation in fission yeast.** Schematic representation of the pVHL protein with the three exons depicted above. Black boxes indicate the three Aggregation-Prone Regions. The P86L mutation favors SDA formation while the P146A mutation promotes large inclusion (LSA) formation. In contrast, the I151S mutation inhibits LSA formation. Pac10 is required for LSA formation. See Discussion for details.

References

Balasubramanian, M. K., McCollum, D. and Gould, K. L. (1997). Cytokinesis in fission yeast Schizosaccharomyces pombe. *Methods Enzymol* **283**, 494-506.

Brock, K. P., Abraham, A. C., Amen, T., Kaganovich, D. and England, J. L. (2015). Structural Basis for Modulation of Quality Control Fate in a Marginally Stable Protein. *Structure* **23**, 1169-78.

Cai, Q. and Robertson, E. S. (2010). Ubiquitin/SUMO modification regulates VHL protein stability and nucleocytoplasmic localization. *PLoS One* **5**.

Cai, Q., Verma, S. C., Kumar, P., Ma, M. and Robertson, E. S. (2010). Hypoxia inactivates the VHL tumor suppressor through PIASy-mediated SUMO modification. *PLoS One* **5**, e9720.

Chesnel, F., Hascoet, P., Gagne, J. P., Couturier, A., Jouan, F., Poirier, G. G., Le Goff, C., Vigneau, C., Danger, Y., Verite, F. et al. (2015). The von Hippel-Lindau tumour suppressor gene: uncovering the expression of the pVHL172 isoform. *Br J Cancer* **113**, 336-44.

Coelho, M., Lade, S. J., Alberti, S., Gross, T. and Tolic, I. M. (2014). Fusion of protein aggregates facilitates asymmetric damage segregation. *PLoS Biol* **12**, e1001886.

Conchillo-Sole, O., de Groot, N. S., Aviles, F. X., Vendrell, J., Daura, X. and Ventura, S. (2007). AGGRESCAN: a server for the prediction and evaluation of "hot spots" of aggregation in polypeptides. *BMC Bioinformatics* **8**, 65.

Ding, Z., German, P., Bai, S., Reddy, A. S., Liu, X. D., Sun, M., Zhou, L., Chen, X., Zhao, X., Wu, C. et al. (2014). Genetic and pharmacological strategies to refunctionalize the von Hippel Lindau R167Q mutant protein. *Cancer Res* **74**, 3127-36.

Escusa-Toret, S., Vonk, W. I. and Frydman, J. (2013). Spatial sequestration of misfolded proteins by a dynamic chaperone pathway enhances cellular fitness during stress. *Nat Cell Biol* **15**, 1231-43.

Feldman, D. E., Spiess, C., Howard, D. E. and Frydman, J. (2003). Tumorigenic mutations in VHL disrupt folding in vivo by interfering with chaperonin binding. *Mol Cell* **12**, 1213-24.

Feldman, D. E., Thulasiraman, V., Ferreyra, R. G. and Frydman, J. (1999). Formation of the VHL-elongin BC tumor suppressor complex is mediated by the chaperonin TRiC. *Mol Cell* **4**, 1051-61.

Fernandez-Escamilla, A. M., Rousseau, F., Schymkowitz, J. and Serrano, L. (2004). Prediction of sequence-dependent and mutational effects on the aggregation of peptides and proteins. *Nat Biotechnol* **22**, 1302-6.

Kaganovich, D., Kopito, R. and Frydman, J. (2008). Misfolded proteins partition between two distinct quality control compartments. *Nature* **454**, 1088-95.

Kamura, T., Sato, S., Iwai, K., Czyzyk-Krzeska, M., Conaway, R. C. and Conaway, J. W. (2000). Activation of HIF1alpha ubiquitination by a reconstituted von Hippel-Lindau (VHL) tumor suppressor complex. *Proc Natl Acad Sci U S A* **97**, 10430-5.

Latif, F., Tory, K., Gnarra, J., Yao, M., Duh, F. M., Orcutt, M. L., Stackhouse, T., Kuzmin, I., Modi, W., Geil, L. et al. (1993). Identification of the von Hippel-Lindau disease tumor suppressor gene. *Science* **260**, 1317-20.

McClellan, A. J., Scott, M. D. and Frydman, J. (2005). Folding and quality control of the VHL tumor suppressor proceed through distinct chaperone pathways. *Cell* **121**, 739-48.

Melville, M. W., McClellan, A. J., Meyer, A. S., Darveau, A. and Frydman, J. (2003). The Hsp70 and TRiC/CCT chaperone systems cooperate in vivo to assemble the von Hippel-Lindau tumor suppressor complex. *Mol Cell Biol* **23**, 3141-51.

Miller, S. B., Ho, C. T., Winkler, J., Khokhrina, M., Neuner, A., Mohamed, M. Y., Guilbride, D. L., Richter, K., Lisby, M., Schiebel, E. et al. (2015). Compartment-specific aggregases direct distinct nuclear and cytoplasmic aggregate deposition. *EMBO J* **34**, 778-97.

Moreno, S., Klar, A. and Nurse, P. (1991). Molecular genetic analysis of fission yeast Schizosaccharomyces pombe. *Methods Enzymol* **194**, 795-823.

Mukaiyama, H., Kajiwara, S., Hosomi, A., Giga-Hama, Y., Tanaka, N., Nakamura, T. and Takegawa, K. (2009). Autophagy-deficient Schizosaccharomyces pombe mutants undergo partial sporulation during nitrogen starvation. *Microbiology* **155**, 3816-26.

Ogrodnik, M., Salmonowicz, H., Brown, R., Turkowska, J., Sredniawa, W., Pattabiraman, S., Amen, T., Abraham, A. C., Eichler, N., Lyakhovetsky, R. et al. (2014). Dynamic JUNQ inclusion bodies are asymmetrically inherited in mammalian cell lines through the asymmetric partitioning of vimentin. *Proc Natl Acad Sci U S A* **111**, 8049-54.

Olzscha, H., Schermann, S. M., Woerner, A. C., Pinkert, S., Hecht, M. H., Tartaglia, G. G., Vendruscolo, M., Hayer-Hartl, M., Hartl, F. U. and Vabulas, R. M. (2011). Amyloid-like aggregates sequester numerous metastable proteins with essential cellular functions. *Cell* **144**, 67-78.

Park, K. S., Kim, J. H., Shin, H. W., Chung, K. S., Im, D. S., Lim, J. H. and Jung, C. R. (2015). E2-EPF UCP regulates stability and functions of missense mutant pVHL via ubiquitin mediated proteolysis. *BMC Cancer* **15**, 800.

Richard, S., Gardie, B., Couve, S. and Gad, S. (2013). Von Hippel-Lindau: how a rare disease illuminates cancer biology. *Semin Cancer Biol* **23**, 26-37.

Saarikangas, J. and Barral, Y. (2015). Protein aggregates are associated with replicative aging without compromising protein quality control. *Elife* **4**.

Schoenfeld, A. R., Davidowitz, E. J. and Burk, R. D. (2000). Elongin BC complex prevents degradation of von Hippel-Lindau tumor suppressor gene products. *Proc Natl Acad Sci U S A* **97**, 8507-12.

Shmueli, M. D., Schnaider, L., Rosenblum, D., Herzog, G., Gazit, E. and Segal, D. (2013). Structural insights into the folding defects of oncogenic pVHL lead to correction of its function in vitro. *PLoS One* **8**, e66333.

Specht, S., Miller, S. B., Mogk, A. and Bukau, B. (2011). Hsp42 is required for sequestration of protein aggregates into deposition sites in Saccharomyces cerevisiae. *J Cell Biol* **195**, 617-29.

Spokoini, R., Moldavski, O., Nahmias, Y., England, J. L., Schuldiner, M. and Kaganovich, D. (2012). Confinement to organelle-associated inclusion structures mediates asymmetric inheritance of aggregated protein in budding yeast. *Cell Rep* **2**, 738-47.

Stickle, N. H., Chung, J., Klco, J. M., Hill, R. P., Kaelin, W. G., Jr. and Ohh, M. (2004). pVHL modification by NEDD8 is required for fibronectin matrix assembly and suppression of tumor development. *Mol Cell Biol* **24**, 3251-61.

Summers, D. W. and Cyr, D. M. (2011). Use of yeast as a system to study amyloid toxicity. *Methods* **53**, 226-31.

Sutovsky, H. and Gazit, E. (2004). The von Hippel-Lindau tumor suppressor protein is a molten globule under native conditions: implications for its physiological activities. *J Biol Chem* **279**, 17190-6.

Tartaglia, G. G., Pawar, A. P., Campioni, S., Dobson, C. M., Chiti, F. and Vendruscolo, M. (2008). Prediction of aggregation-prone regions in structured proteins. *J Mol Biol* **380**, 425-36.

Tsuchiya, H., Iseda, T. and Hino, O. (1996). Identification of a novel protein (VBP-1) binding to the von Hippel-Lindau (VHL) tumor suppressor gene product. *Cancer Res* **56**, 2881-5.

Tyedmers, J., Mogk, A. and Bukau, B. (2010). Cellular strategies for controlling protein aggregation. *Nat Rev Mol Cell Biol* **11**, 777-88.

Weisberg, S. J., Lyakhovetsky, R., Werdiger, A. C., Gitler, A. D., Soen, Y. and Kaganovich, D. (2012). Compartmentalization of superoxide dismutase 1 (SOD1G93A) aggregates determines their toxicity. *Proc Natl Acad Sci U S A* **109**, 15811-6.

Yang, C., Huntoon, K., Ksendzovsky, A., Zhuang, Z. and Lonser, R. R. (2013). Proteostasis modulators prolong missense VHL protein activity and halt tumor progression. *Cell Rep* **3**, 52-9.
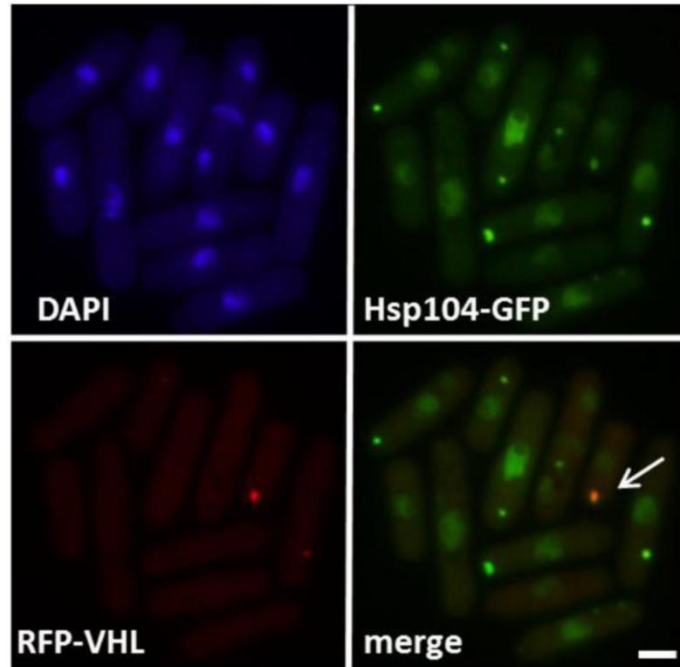
Figure S1: RFP-tagged pVHL colocalizes with Hsp104-GFP.
Hsp104-GFP fission yeast cells that overexpress RFP-VHL213 were fixed and stained with DAPI.
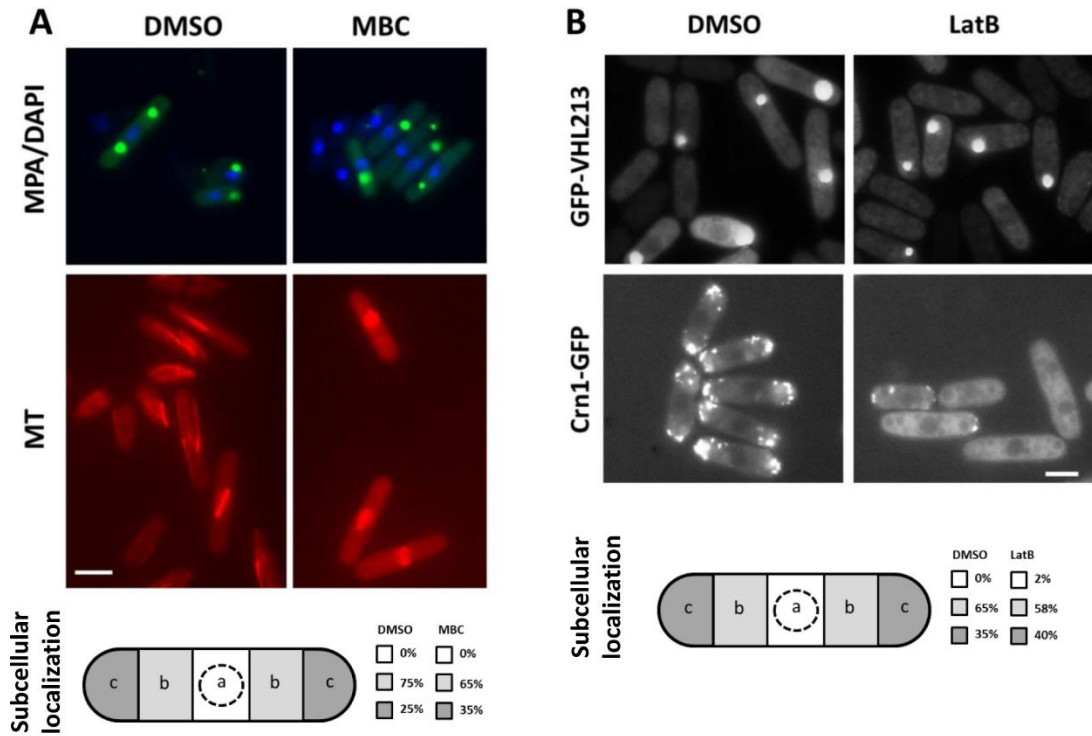Arrow in merge shows an inclusion that contains both RFP-VHL213 and Hsp104-GFP. Bar: 5 μm.

Figure S2

A) The microtubule network does not regulate LSA formation or localization.

In cells overexpressing GFP-VHL213, microtubules (MT) were depolymerized with
25 mg/ml Methyl benzimidazol-2-yl-carbamate (MBC) or DMSO (control) for 1h
and stained with DAPI (upper panels). Disruption of the MT network by MBC was
ascertained using an alpha-tubulin mCherry-Atb2 expressing strain
(*h+ hphMX6:nmt81:mCherry-atb2 ura4-D18 ade6-210 leu1-32*, Table S3)
in parallel (lower panels). Bar: 5 μm. The bottom scheme shows the subcellular localization
of GFP-VHL213 LSA in DMSO- (n=253) or MBC-treated (n=95) cells. GFP-VHL213
overexpressing cells were divided into five segments of the same size and the percentage
of cells with LSA in the different segments was calculated. The nucleus is indicated by a dashed
circle in the schematic representation of the cell.

B) The F-actin cytoskeleton does not regulate LSA formation or localization.

The F-actin cytoskeleton was depolymerized or not (DMSO) in cells overexpressing
GFP-VHL213 with 20 μM Latrunculin B (LatB) for 30 minutes (upper panels).
F-actin cytoskeleton depolymerization with LatB was ascertained using a strain that express
GFP-tagged coronin (Crn1-GFP, lower panels, Table S3). In control cells (DMSO),
coronin bright polarized signal marks the F-actin patches at cell ends. Upon F-actin
depolymerization by LatB, the signal becomes diffuse. Bar: 5 μm. The bottom scheme shows
the subcellular localization of GFP-VHL213 LSA in DMSO- (n=79) or LatB-treated (n=118) cells.
GFP-VHL213 overexpressing cells were divided into five segments of the same size and the percentage
of cells with LSA in the different segments was calculated. The nucleus is indicated by a dashed
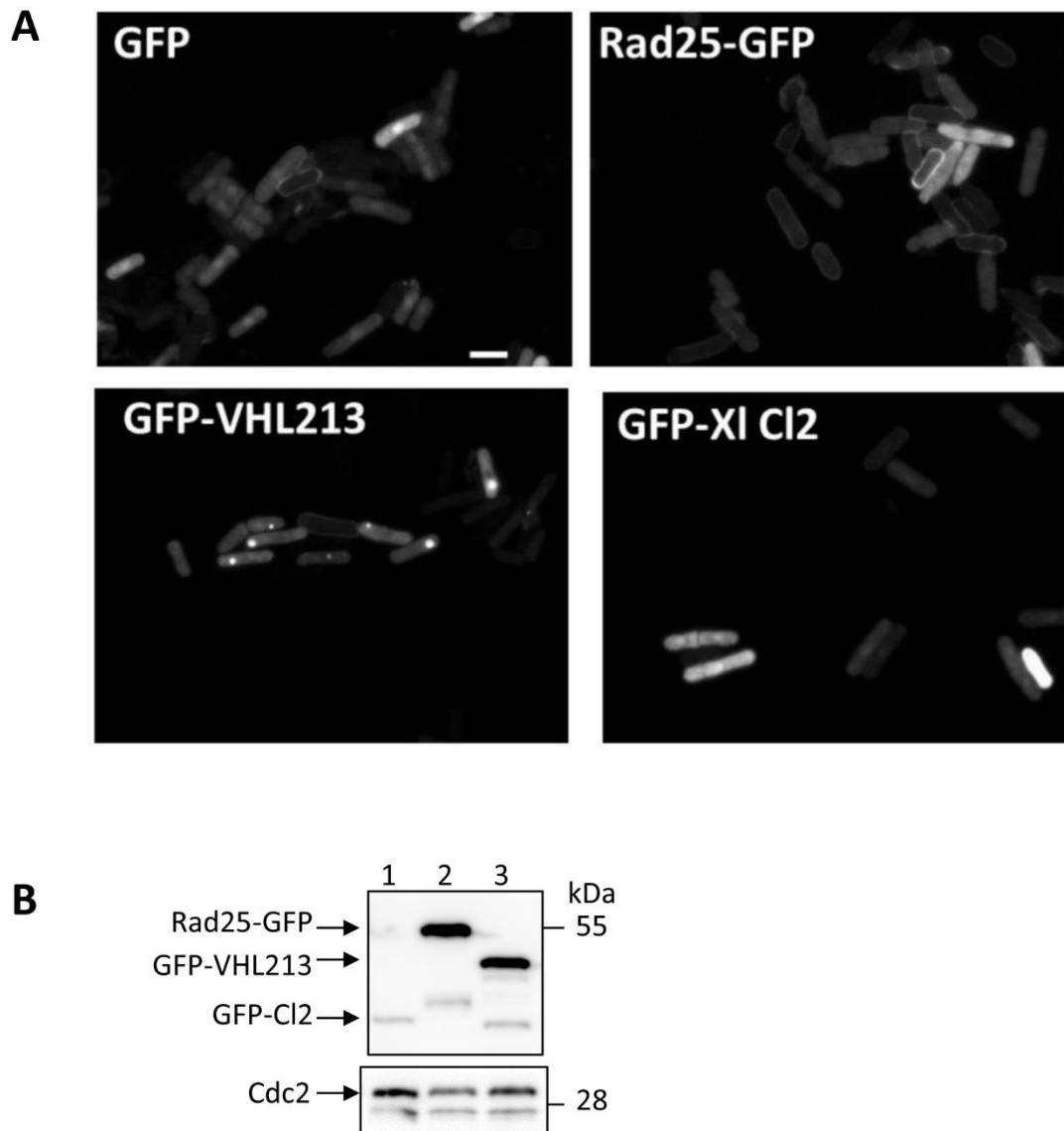circle in the schematic representation of the cell.

A

B

Figure S3: GFP alone or GFP-tagged control proteins do not form cytoplasmic inclusions when overexpressed in fission yeast cells.

The fission yeast Rad25-GFP (270 amino acids) and *Xenopus laevis* Cl2 (102 amino acids, *Xl* Cl2) proteins were chosen because they exhibit a similar percentage of hydrophobic residues (23.4% and 25.5%, respectively) as pVHL213 (24.8%). Rad25-GFP and GFP-Xl Cl2 expression was under the control of the *nmt41* promoter (Table S1). A) Cells overexpressing GFP alone (empty vector) or the different GFP-tagged proteins after 16h induction were imaged with a Leica DMRXA2 microscope. Only GFP-VHL213 cells (33% of all cells) formed cytoplasmic inclusions. Bar: 10 μm. B) Western blot analysis of the expression of the GFP-tagged proteins after 16h induction probed with an anti-GFP antibody (upper panel, lane 1: GFP-Xl Cl2, lane 2: Rad25-GFP, lane 3: GFP-VHL213) and with anti-Cdc2 (lower panel). Cdc2 expression was used as a loading control.

Figure S4: Hydrophobicity profiles of wild type and mutant pVHL using TANGO.
The ORF sequences of the different pVHL213 were analyzed with the TANGO software
(www.switchlab.org/bioinformatics/tango). The TANGO scores of individual residues were plotted
as a function of their position in the pVHL ORF. In wild type pVHL (upper left panel; WT), three
Aggregation Promoting Regions (APR) were identified (APR1, APR2 and APR3). The P86L mutation
strikingly enhanced the aggregation propensity of APR1 and APR2 by fusing them (upper right
panel). The P146A mutation extended the APR3 region and increased its score by two-fold (lower
left panel). In contrast, I151S abolished APR3 aggregation propensity (lower right panel).

Supplementary Table S1: Plasmids used in this study

Plasmid	Promoter	Expressed gene product
pREP1-VHL213	nmt1	pVHL213
pSLF279-VHL213	nmt41	RFP-VHL213
pREP1-VHL160	nmt1	pVHL160
pREP1-VHL172	nmt1	pVHL172
pREP41-GFP-VHL160	nmt41	GFP-VHL160
pREP41-GFP-VHL172	nmt41	GFP-VHL172
pREP41GFP-VHL213	nmt41	GFP-VHL213
pREP41GFP-XlCl2	nmt41	GFP-Cl2
pREP41-Rad25-GFP[a]	nmt41	Rad25-GFP
pREP41GFP-VHL213 3KR	nmt41	GFP-VHL213 3KR
pREP41GFP-VHL213 P86L	nmt41	GFP-VHL213 P86L
pREP41GFP-VHL213 P146A	nmt41	GFP-VHL213 P146A
pREP41GFP-VHL213 I151S	nmt41	GFP-VHL213 I151S

[a] a kind gift of M. Kawamukai (Japan)

Supplementary Table S2: Percentage of cells showing one or two Hsp104-GFP dots
and mean size of Hsp104-GFP dots in *hsp104-GFP* cells transformed with empty vector
(pREP1) or the pREP1-VHL213 plasmid (pVHL213) that were cultured in the ON
condition for 16h and then in the OFF condition for 8h (mean values of three independent
experiments±s.d).

Plasmid	ON/OFF 8h	1 dot (% cells)	2 dots (% cells)	mean size (μm^2)	n
pREP1	ON	46.1±8.0	9.5±7.6	0.25±0.13	87
pREP1	OFF 8h	46.2±3.3	9.2±6.5	0.28±0.20	102
pVHL213	ON	44.6±8.6	28.2±5.9	0.58±0.37	76
pVHL213	OFF 8h	40.8±2.2	5.5±5.1	0.30±0.24	97

Supplementary Table S3: The aggregation propensity of pVHL mutants given as percentage of the overall aggregation score of wild type pVHL using three different algorithms.

Missense mutants of pVHL were analyzed with three algorithms for aggregation propensity prediction (TANGO, Zyggregator and Aggrescan). The score of wild type pVHL was set as 100%. Blue: score <95% (lower aggregation propensity); red: score >105% score (higher aggregation propensity than wild type).

	TANGO	Zyggregator	Aggrescan
WT	100.0	100.0	100.0
S65W	100.0	101.4	105.5
F76S	87.8	75.4	88.2
N78H	98.6	99.8	101.8
N78Y	321.6	101.8	116.3
N78S	106.8	100.0	106.7
S80R	98.6	94.4	95.5
P86L	1220.3	118.7	134.2
W88C	79.7	104.0	98.0
L89R	78.4	94.9	82.4
L89H	78.4	98.4	82.4
G93R	250	95.0	82.4
Y112N	100.0	99.4	100.0
G114R	100.0	97.8	100.0
H115N	133.8	100.3	100.0
W117R	100.0	100.5	100.0
D121Y	98.6	110.2	125.9
P146A	140.5	107.7	103.5
I151S	55.4	95.7	85.9
T152P	55.4	95.2	85.9
V155L	98.6	97.4	98.4
L158V	102.7	99.4	101.0
L158P	97.3	102.2	87.1
E160V	93.2	104.8	126.5
C162W	152.7	99.4	104.9
Q164P	95.9	103.0	107.8
Q164K	95.9	102.7	103.9
V166G	95.9	101.0	90.0
K171R	100.0	100.0	99.1

Supplementary Table S4: Strains used in this study.

Number	Genotype	Reference
XLG029	*h- leu1-32*	Lab stock
DN111	*h- hsp104-GFP-S65T:kan*	(Nilsson and Sunnerhagen, 2011)
XLG841	*h- leu1-32 ade6- ura4-D18 hsp104-GFP-S65T:kan*	This study
PN4751	*h+ Amo1-MRFP1::kanMX6 SV40-GFP-atb2::LEU2*	(Pardo and Nurse, 2005)
XLG967	*h- amo1-RFP::kanMX6 leu1-32 ura4-D18*	This study
XLG473	*h+ crn1-GFP-kanMX ade6- leu1-32 ura4-D18*	(Pelham and Chang, 2001)
KS2789	h+ hphMX6:nmt81:mCherry-atb2 ura4-D18 ade6-210 leu1-32	(Snaith et al., 2005)
SK1	*h- leu1-32 ura4-C190T atg1::ura4+*	(Mukaiyama et al., 2009)
XLG822	*h- mts3-1 ade6- ura4-D18 leu1-32*	A kind gift of C. Gordon (UK)
XLG939	*h+ pac10::kanR ura4-D18 ade6-M210 leu1-32*	A kind gift of P. Sunnerhagen (Sweden)
MC135	*h- hsp16::ura4+ hsp104-GFP-kanR ura4-D18*	(Coelho et al., 2014)
XLG982	*h- hsp16::ura4+ leu1-32 ura4-D18*	This study

Coelho, M., Lade, S. J., Alberti, S., Gross, T. and Tolic, I. M. (2014). Fusion of protein aggregates facilitates asymmetric damage segregation. *PLoS Biol* **12**, e1001886.

Mukaiyama, H., Kajiwara, S., Hosomi, A., Giga-Hama, Y., Tanaka, N., Nakamura, T. and Takegawa, K. (2009). Autophagy-deficient Schizosaccharomyces pombe mutants undergo partial sporulation during nitrogen starvation. *Microbiology* **155**, 3816-26.

Nilsson, D. and Sunnerhagen, P. (2011). Cellular stress induces cytoplasmic RNA granules in fission yeast. *RNA* **17**, 120-33.

Pardo, M. and Nurse, P. (2005). The nuclear rim protein Amo1 is required for proper microtubule cytoskeleton organisation in fission yeast. *J Cell Sci* **118**, 1705-14.

Pelham, R. J., Jr. and Chang, F. (2001). Role of actin polymerization and actin cables in actin-patch movement in Schizosaccharomyces pombe. *Nat Cell Biol* **3**, 235-44.

Snaith, H. A., Samejima, I. and Sawin, K. E. (2005). Multistep and multimode cortical anchoring of tea1p at cell tips in fission yeast. *EMBO J* **24**, 3690-9.

Supplementary Table S5 : List of PCR-primers used in this study.
The *Nde*I and *BamH*I restriction sites are shown in italics (in VHL1S/2S and 3AS, respectively); mutated nucleotides are underlined.
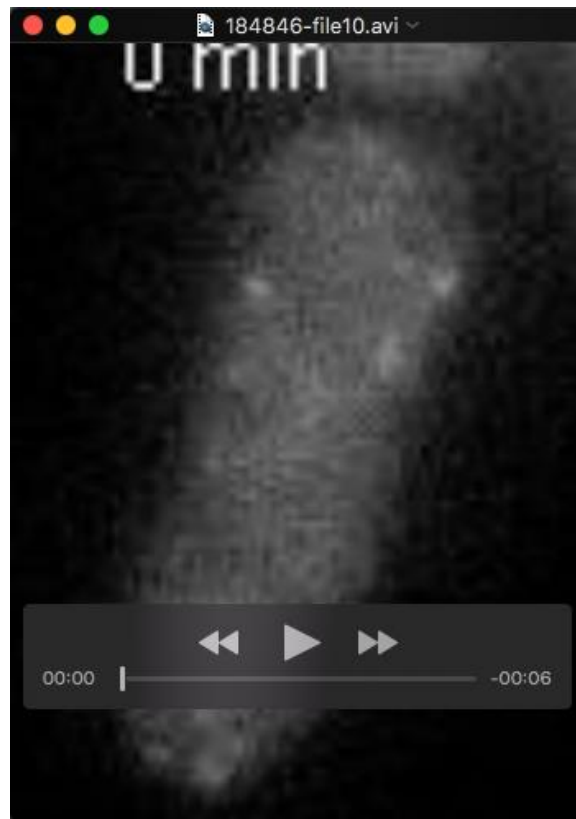
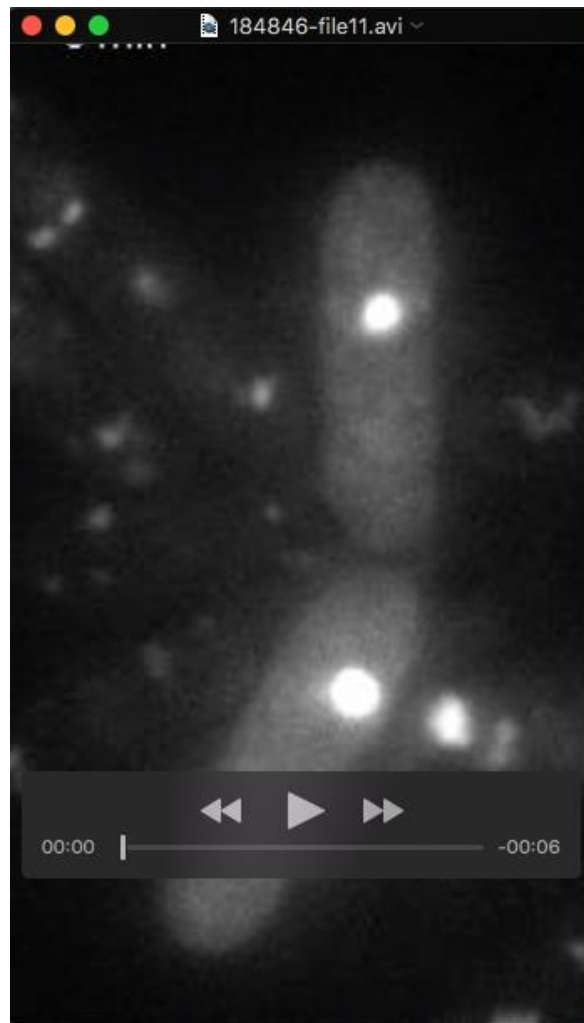| Primer name	Primer sequence (5' … 3')
VHL1S	*CATATG*CCCCGGAGGGCGGAGAACT
VHL2S	*CATATG*GAGGCCGGGCGGCCGCGGC
VHL3AS	*GGATCC*TCAATCTCCCATCCGTTGA
VHL11SalIS	GCTTTGTCGACTCATATGCCCCGGA
VHL13SmaIAS	TTACCCGGGGATCCTCAATCTC
P86LFor	TGCTCGTATGGCTCAACTTCGACGG
P86LRev	TGAGCCATACGAGCAGCACGACGCG
P146AFor	GTTGACGGACAG<u>G</u>CTATTTTTGCCA
P146ARev	TGGCAAAAATAG<u>C</u>CTGTCCGTCAAC
I151SFor	GCCAATA<u>G</u>CACACTGCCAGTGTATAC
I151SRev	GTATACACTGGCAGTGTG<u>C</u>TATTGGC
K159RFor	TATACTCTGA<u>G</u>AGAGCGATGCC
K159RRev	GGCATCGCTCT<u>C</u>TCAGAGTATA
K171RFor	GAGCCTAGTCA<u>G</u>GCCTGAGAATT
K171RRev	AATTCTCAGGC<u>C</u>TGACTAGGCTC
K196RFor	AAATGTGCAGA<u>G</u>AGACCTGGAG
K196RRev	CTCCAGGTCT<u>C</u>TCTGCACATTT

Movie 1: Dynamics of SDA. GFP-VHL213 expressing cells were imaged every 5 seconds (Leica DMRXA). Note that extensive photobleaching was observed.

Movie 2: LSA shows limited movements within the cell. GFP-VHL213 expressing cell was imaged every 2 minutes (Leica DMIRB).

Movie 3: LSA formation. Two LSA are present in the cell and one is formed *de novo* in the top of the cell (from t30 to t60 min.). GFP-VHL213 cell was imaged every 5 minutes (Leica DMIRB).

Movie 4: LSA disappearance. Two cells each with one LSA showed disappearance of LSA: in 30 min. (upper cell) or 50 min. (lower cell). GFP-VHL213 cells were imaged every 5 minutes (Leica DMIRB).

Movie 5: Small puncta and inclusion dynamics of GFP-VHL160. Two GFP-VHL160 expressing cells were imaged every 1 second. Both cells showed highly dynamic small puncta and the upper cell contains an immobile inclusion (Nikon spinning disk).